

CHAPTER 4:

FABRICATION OF SUPERCONDUCTING TAPES BY DEPOSITING NdBCO FILMS ON BIAXIALY TEXTURED NICKEL

4.1 Background

This chapter discusses the method used for fabricating rolling-assisted-biaxially-textured substrates (RABiTS) by pulsed-laser deposition of oxides buffer-layers on textured nickel. It also presents the results obtained by depositing NdBCO and YBCO superconductors on RABiTS by PLD.

The deposition of a buffer layer is the first step required in deposition of a ceramic superconductor on a metal substrate. Its role is mainly to overcome diffusion problems between the substrate and the superconducting layer, and formation of oxides at their interface. However, physical vapor deposition on a polycrystalline substrate results only in an uniaxial orientation of the buffer layer along the perpendicular to the surface, while the in-plane axes are randomly oriented. Consequently, the superconducting layer deposited on top of the buffer layer does not show biaxial texture. Biaxial texture of the buffer layer was achieved for the first time by Iijima et al. [41] and Reade et al. [42] who independently used a technique called ion-beam-assisted-deposition (IBAD). Such a technique consists

of bombarding the growing film with an ion beam oriented along a specific angle with respect to the substrate normal (54.7° in the case of YSZ), depending on the ceramic's crystal structure and the desired orientation. Channelling of the ions in the specified lattice direction allows the growth of only one orientation, while the crystallites having different orientations are ablated away as they grow. The grains of the desired orientation grow faster than the others, and ultimately shadow and extinguish completely the crystallites with different orientations [43]. Since a predominant fraction of the material deposited is removed by the impinging ions, this technique is limited by a very slow deposition rate and was not generally considered as a promising, industrial-scalable approach when proposed.

4.2 The second generation of HTS conductors: the RABiTS substrate

The superconductivity group of Oak Ridge National Laboratory has recently developed a new approach for depositing HTS films on a metallic tape without using an additional ion source during the growth process. The first step of this method is to obtain a very sharp cube texture for Nickel tapes by thermo-mechanical processing of the metal. A high purity (99.99%) polycrystalline bar of Ni is cold rolled to total deformation greater than 90% and subsequently annealed in vacuum ($\sim 10^{-6}$ Torr) in a wide temperature range for recrystallization. The result is the formation of a sharp biaxial cubic texture, with typical full-width-half-maximum values for X-ray ω - and ϕ -scans of 6° and 7° . Polishing of the Ni surface is avoided by controlling the surface conditions of the work rolls. In this way it is possible to obtain very smooth surfaces ($\text{rms} \approx 10$ nm) adequate for film growth, with an average grain size of $100 \mu\text{m}$. Calculations of the grain boundary

misorientation angles are conducted at ORNL using backscattered electron Kikuchi diffraction (BKD) [46]. The results of such analysis on Ni textured substrates typically show that most of the boundaries have misorientation angles in the range 1 - 5° and most of the substrate is percolatively connected within 5°.

The second step of this process involves deposition on the metal of a buffer layer that is chemically and structurally adequate for subsequent growth of high quality epitaxial superconducting films. The best buffer layers for YBCO film growth are oxides, and these materials are normally deposited in the presence of an oxygen background pressure. On the other hand, a Ni surface reacts very easily with O₂, forming a (111) textured NiO layer, the orientation of which is unsuitable for fabricating high-J_c HTS films because many high angle boundaries are present. This problem can be overcome by two methods. The first, which employs deposition of less reactive noble metal layers on Ni to prevent NiO formation, followed by deposition of oxides, will not be discussed in this work. The second method, which has provided the best results, employs deposition of oxides directly on Ni under reducing condition. Different vapor deposition techniques (e-beam, sputtering, PLD, precursor YBCO method) are used at ORNL to deposit both buffer layers and YBCO on Ni. The choice of deposition technique is dictated by the film quality provided, but also by the optimization of the deposition rate and the industrial scalability of the equipment. At present, the best film properties in the case of complex materials like HTS are obtained using PLD, while different techniques have been equally successful for depositing oxide buffer layers.

The work presented here is focused on the use of PLD. Consequently, both buffer layer architecture and the superconducting layer were deposited using this technique, following a process previously optimized for YBCO. The purpose of the buffer layer is to retard oxidation of Ni, to reduce the lattice mismatch

between Ni and the cuprate superconductors, and to prevent diffusion of Ni into YBCO. Previous experimental studies on the growth of epitaxial oxide buffer layers on Ni indicated that CeO₂ was a good candidate. Growth of CeO₂ on Ni results in the single (100) epitaxial orientation, when a particular procedure is used in depositing the oxide. During the substrate heating phase, a mixture of 96% Ar and 4% H₂ is introduced in the vacuum system. The flow is regulated to obtain a total pressure [P(Ar) + P(H₂)] of 100 - 200 mTorr. The presence of the reducing gas protect the Ni surface from the formation of NiO. Since Ni surface oxidation increases with temperature, the CeO₂ is deposited at the relatively low substrate temperature of 600 °C. A former thin layer formed by 300 laser shots of CeO₂ is deposited in the same background mixture of Ar and H₂, using a laser energy of 300 mJ/shot and a repetition rate of 3 Hz. A subsequent layer formed by nearly 500 shots is then deposited after the chamber is pumped out, in a residual vapor pressure of 10⁻⁶ Torr. In this way, the Ni surface is covered with a 400 Å thick film which prevents Ni oxidation during the rest of the process. At this point, oxygen is introduced in the chamber to a pressure of 1 x 10⁻⁴ Torr, and growth of the CeO₂ layer is concluded by depositing a ~4600 Å thick layer at T_s=600 °C using the same laser beam energy and increasing the repetition rate to the value of 10 Hz. The (100) oriented CeO₂ layer provides a template for subsequent epitaxial growth of another buffer-layer or the ceramic superconductor. Although cerium-oxide is an optimal buffer layer for epitaxial growth of HTS, the high oxygen diffusion through CeO₂ could still lead to the formation of NiO at the metal interface when depositing cuprate-oxides superconductors that require background oxygen pressures of hundreds of mTorr. Moreover, due to the stress created by the lattice mismatch and the difference in the thermal expansion between substrate and buffer layer, the CeO₂ layer has a high tendency to form cracks. A second buffer layer of yttria-

stabilized-zircon (YSZ) 5000 Å thick is deposited in-situ right after CeO₂ growth at the substrate temperature of 710 °C. YSZ is harder than CeO₂, and more resistant to the formation of cracks. In fact, besides providing a barrier to oxygen diffusion, the YSZ layer seems to alleviate the cracks that are formed underneath. This structure, formed by an epitaxial buffer layer suitable for HTS deposition on the Ni textured substrate, is referred to as RABiTS, the acronym for rolled-assisted-biaxially-textured-substrates.

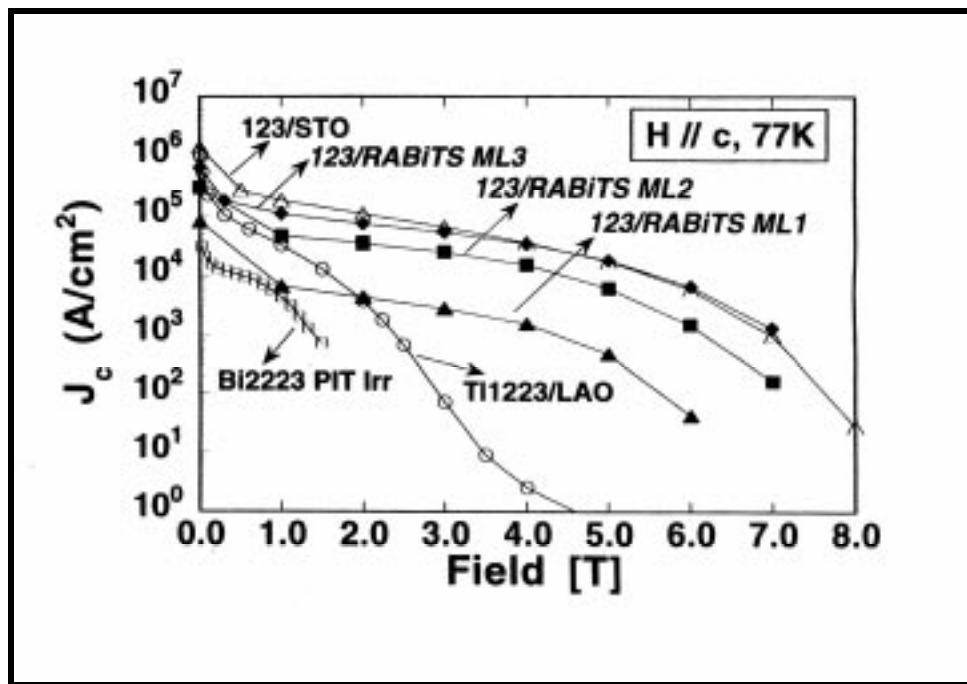


Fig. 4.1. Field dependence of J_c for YBCO on SrTiO₃ (STO) and YBCO on RABiTS substrate of different configurations: CeO₂/Ag/Pd/Ni (ML1), YSZ/CeO₂/Pd/Ni (ML2), YSZ/CeO₂/Ni (ML3). For comparison, J_c field dependence for a Tl-1223 film and a Bi-2223 OPIT sample are reported.

YBCO is the only cuprate-oxide that has been deposited on RABiTS structures thus far. In fact, YBCO has been the widest studied superconductor since the

discovery of High- T_c superconductivity, and so far seems to offer the best performance for application at 77 K. Moreover, at present, high quality epitaxial YBCO films are obtained at ORNL by using a method involving deposition of precursor layers. This method has the advantage of depositing the superconducting layer at low temperature, and, consequently, is more adequate to an industrial developing of coated conductors technology. Figure 4.1 shows a

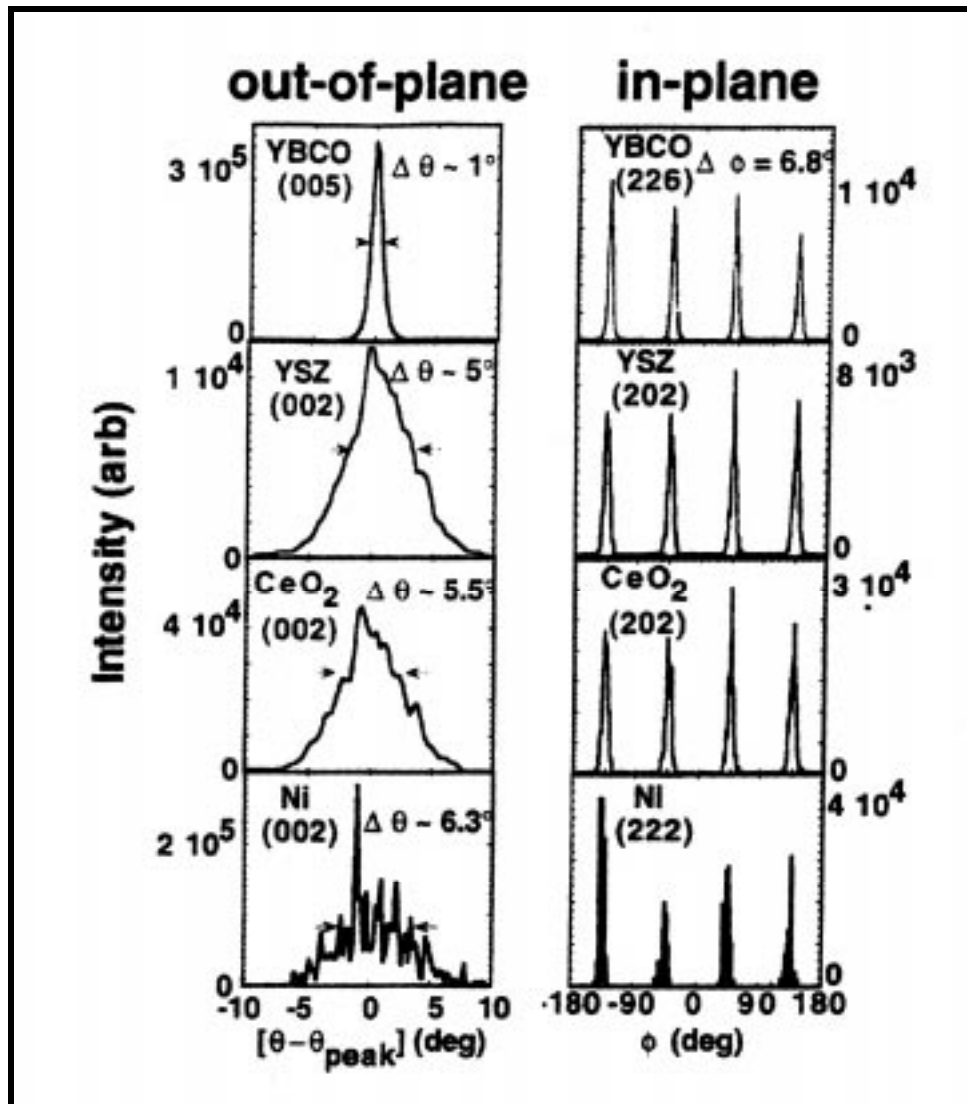


Fig. 4.2. *In-plane and out-of plane texture for YBCO/YSZ/CeO₂/Ni.*

comparison among the field dependence of J_c in YBCO on RABiTS samples (with different architectures), the J_c field dependence measured for YBCO on SrTiO_3 , an epitaxial Tl-1223 film on LaAlO_3 , and Bi-2223/Ag OPIT samples in which additional pinning sites were introduced by proton irradiation.

A typical x-ray θ - 2θ characterization of the YBCO/YSZ/CeO₂/Ni structures reveals that CeO₂ and YSZ buffer-layers are (001) oriented with respect to the surface normal. The rocking curves for the CeO₂ (002) and YSZ (002) peaks show typical FWHMs of 5.5 and 5, respectively. The out-of-plane texture of YBCO shows a significant improvement with respect to the buffer layers with a FWHM of only 1 for the rocking curve of the (005) peak. The in-plane texture revealed by XRD ϕ -scan through orientations other than (001) also indicates excellent epitaxy of the buffer layers on the metal substrate (see Fig. 4.2). The in-plane axes of CeO₂ and YSZ are rotated 45° with respect to the Ni (001) axis, while YBCO grows with a and b axes rotated 45° with respect to YSZ. The normally cubic YSZ and CeO₂ lattices show a small tetragonal distortion with $a = b = 5.41$, $c = 5.422$ for CeO₂, and $a = b = 5.12$, $c = 5.162$ for YSZ. The ratio between the intensities of the CeO₂ (111) peak and the CeO₂ (002) peak in the x-ray spectra is less than 10^{-2} , indicating only a very small volume percentage of (111) oriented oxide.

4.3 Deposition of NdBCO films on RABiTS substrates: a comparison between NdBCO and YBCO

In the work presented here, for the first time we report the results obtained by depositing a superconducting layer of NdBCO on RABiTS substrates. NdBCO was deposited by PLD on a CeO₂/YSZ/CeO₂/Ni architecture. All three layers

were deposited continuously in the same run, without breaking the vacuum conditions. The first layer of CeO₂ and the YSZ layer were deposited using the procedure discussed in the previous paragraph. The only difference being that, after increasing the substrate temperature to the value of 710 °C, and before starting to grow YSZ, we deposited 150 Å of CeO₂ at this temperature to improve the epitaxial relation between the oxides. The final CeO₂ cup layer is introduced to avoid growth of two different in-plane orientations of the superconductor on the YSZ layer, as sometimes is observed for YBCO on RABiTS. In fact, it is known that YBCO can grow with two different epitaxial orientations on YSZ: with <100> or <010> axes aligned with YSZ <100> axis, or with <100> or <010> axes aligned with YSZ <110> axis. This layer was grown in an oxygen background of 1x10⁻⁴ Torr, with a substrate temperature in the range of 710 to 780 °C and a thickness of nearly 100 Å. The NdBCO layers were grown following the exact procedure used for NdBCO films on single crystals, at an oxygen pressure of 0.8 mTorr and a substrate temperature of 780 °C. The films were cooled in the same oxygen partial pressure used for the deposition, and oxygen was introduced in the vacuum chamber (up to a pressure of 500 Torr) only after the substrate temperature had reached the value of 500 °C. Because of the differences in the phase stability relations between NdBCO and YBCO, the NdBCO film is deposited using a background oxygen pressure nearly two orders of magnitude lower than that used for YBCO. This significant difference is interesting because the reduced oxygen pressure might be highly beneficial in preventing the oxidation of nickel. The NdBCO films were formed by 6000 laser shots at the repetition rate of 2 Hz and laser beam energy of 300 mJ/shot, corresponding to a thickness of ~ 0.4 μm. The NdBCO films were shiny and optically smooth like a typical good YBCO film on RABiTS. The nickel substrates, fabricated at Oak Ridge National Laboratory, had dimensions of

10 x 10 mm or 3 x 20 mm, and a thickness of 125 μm . For comparison, YBCO films were deposited on RABiTS substrates using the same buffer-layers growth procedure and architecture, and the optimal growth conditions previously determined for YBCO in the same deposition system.

Critical temperature was evaluated by measuring the resistance-versus-temperature curve with the same four-probe technique discussed for films on single crystals. In this case, the normal-state resistivity is not very meaningful, as shorts between the superconducting layer and the Ni substrate are often present. T_{c0} values observed in YBCO films ranged between 88 and 89.5 K, while NBCO films exhibited typical T_{c0} 's of 92.5-93 K, in accordance with the values reported for optimal NdBCO films on single crystal (see Fig 4.3). Thus, NdBCO films

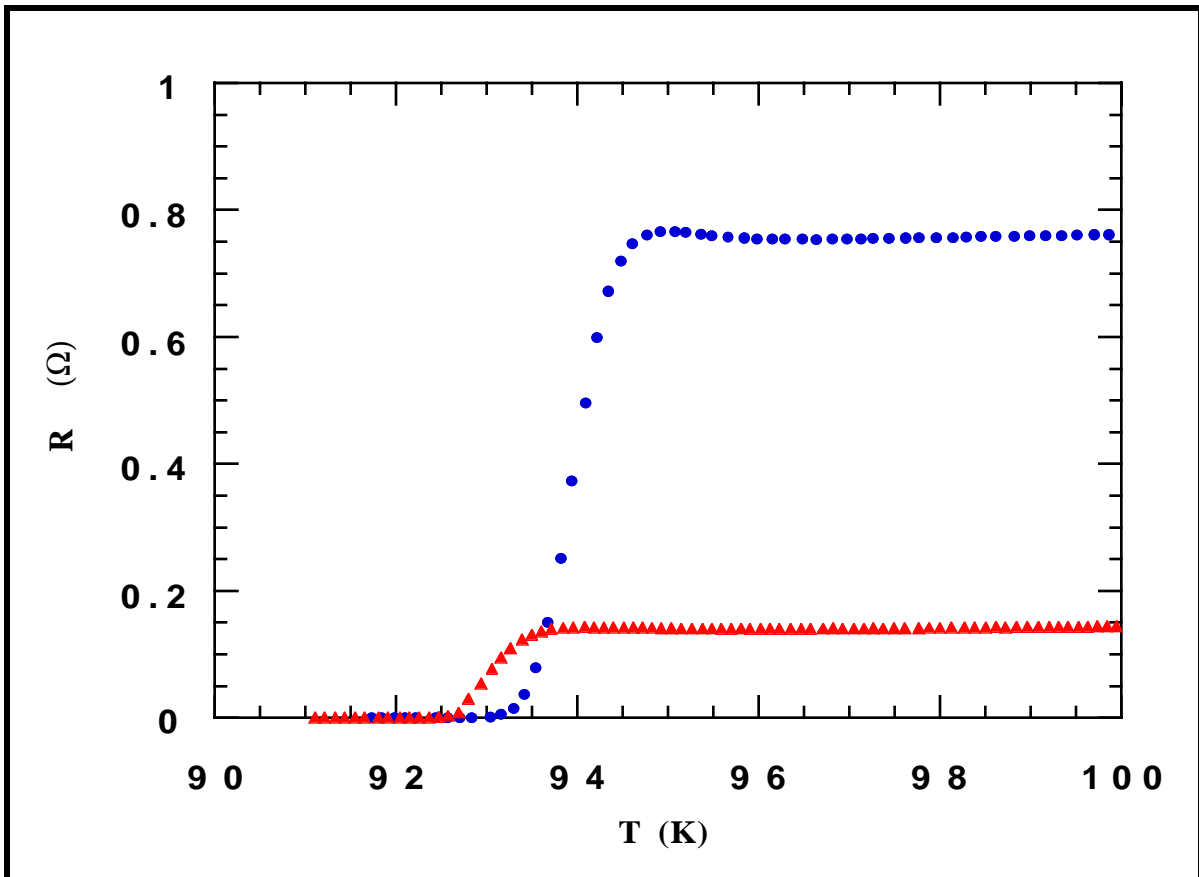


Fig. 4.3. *Resistive transition for the NdBCO samples la062498Ni1 and la0624Ni4.*

deposited on RABiTS, as well as on single crystals (LaAlO₃), showed higher critical temperature than YBCO films on the corresponding substrates.

Structural and morphological characterization.

Structural and morphological characterization of the NdBCO films on RABiTS substrates was conducted using a scanning electron microscope (SEM) equipped for performing backscattered electron diffraction.

When the incident beam electrons in a SEM strikes the surface of a specimen under observation, a significant fraction of them re-emerge from the sample, propagating in the same hemisphere as the original beam. These electrons are called backscattered because they suffer one or more elastic scattering events in which the electron trajectory is changed by more than 90° from the forward direction of motion. The backscattered electrons provide an extremely useful signal for sample characterization, giving at the same time information about composition, local topography, morphology, and crystallography. The fraction of backscattered electrons can be greatly increased by increasing the tilt angle, which is defined as the complement of the angle between the beam and the surface plane. At very high tilt angles (>70°), which correspond to grazing incidence, the number of backscattered electrons approaches the number of incident beam electrons. This behavior originates because of the higher probability of scattering events resulting in small deviation angles. Therefore, when the beam is set almost parallel to the sample's surface, most of the elastically scattered electrons tend to propagate along trajectories near the surface and,

consequently, can escape with less total angular deviation as the result of a much more probable event. When the surface is tilted, the same tendency for forward elastic scattering favors backscattering in the direction away from the incident beam. Consequently, the angular distribution of the backscattered electrons, which at 0° tilt follows a cosine law, becomes very asymmetrical, resembling a highly elongated ellipse, with the long axis forming approximately the same angle with the surface as the beam (see Fig.4.6) [47]. Among the electrons emitted, particularly interesting are those that leave the surface promptly, after very few scattering events, and in the immediate vicinity of the beam impact area. In fact,

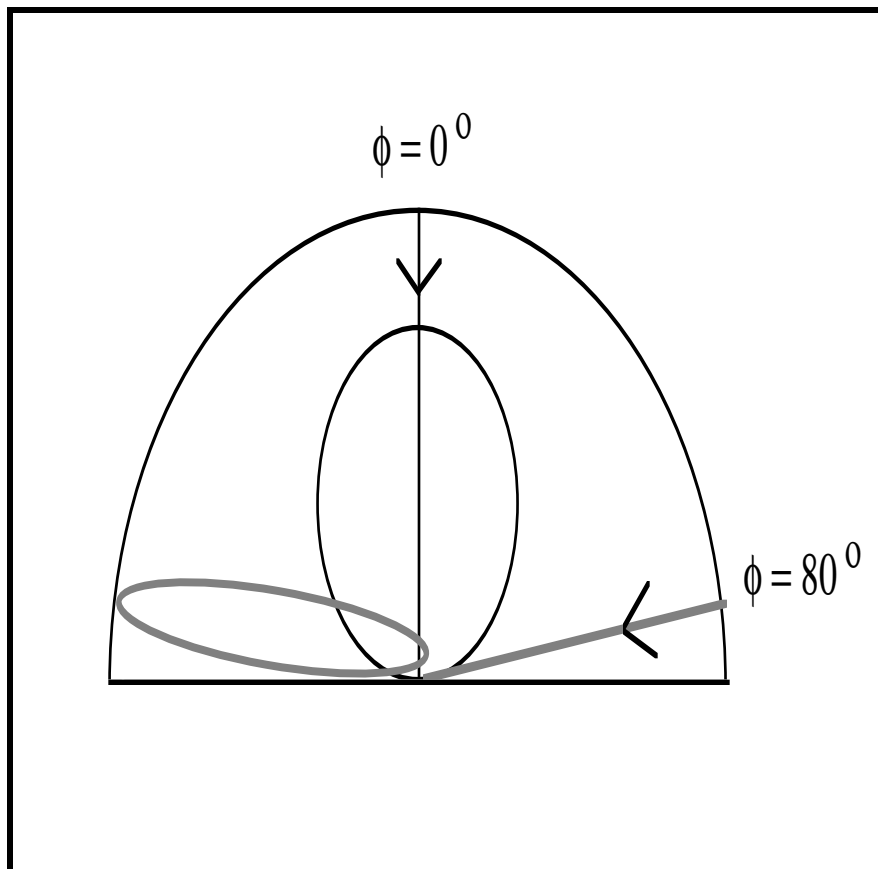
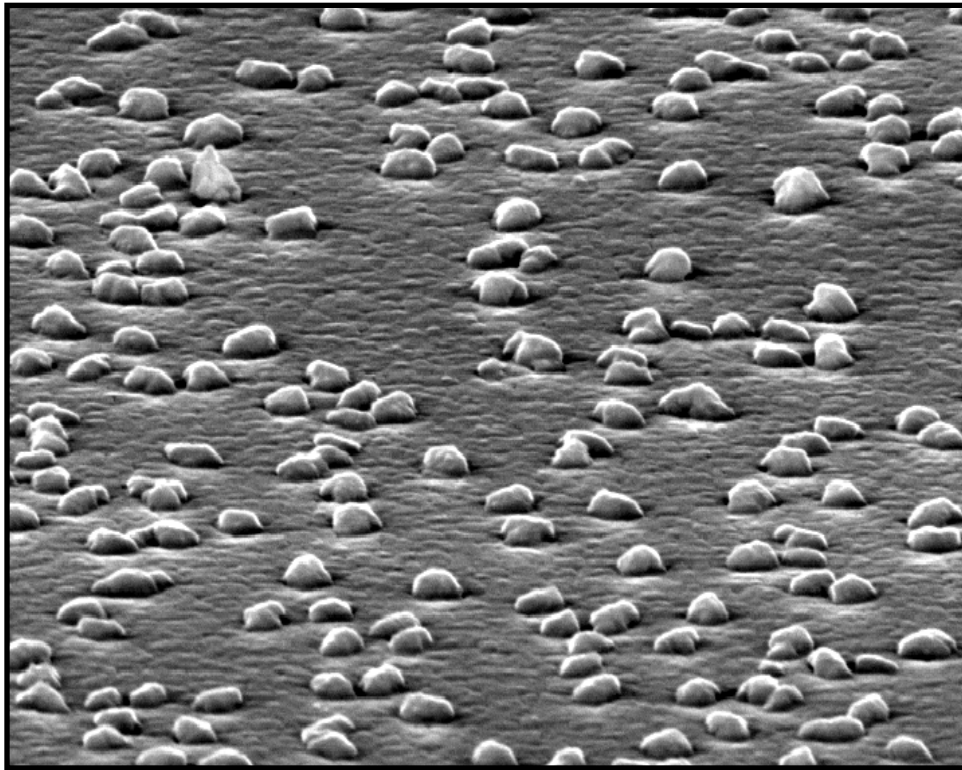


Fig. 4.6. Comparison of the angular distribution of backscattered electrons for sample tilts of $\phi = 0^\circ$ and $\phi = 80^\circ$.

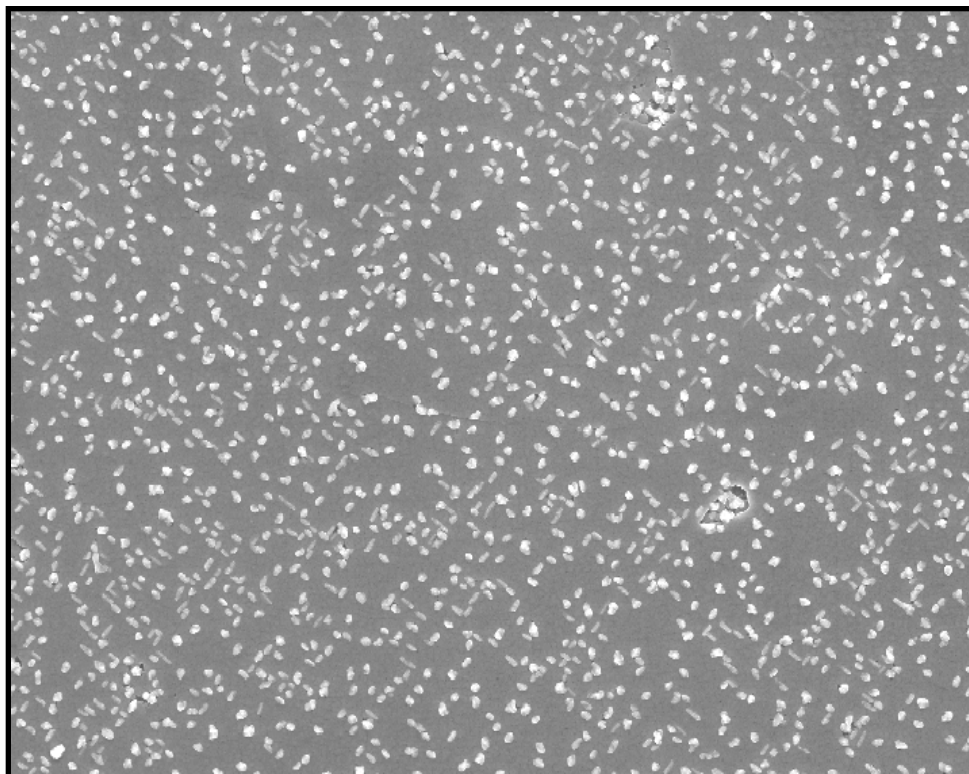
these electrons, which retain almost all the initial energy, constitute a source of high resolution local information about the sample. The fraction of these electrons can be increased by taking advantage of the highly directional distribution originated at high-tilt angles and placing an energy-filtering collector at a low take off angle to the surface. The signal obtained in this way is very sensitive to fine-scale details, with dimensions close to those of the focused probe, and retains information from a thickness of only 10-20 nm from the surface.

Backscattered electron diffraction was used to study the microstructure of the NdBCO film deposited on RABiTS, whose J_c dependence on H is reported in Fig.4.4 (sample 1a062498Ni1). The measurements were performed by scanning the electron beam over several macroscopic regions with a step size of 0.5 micron, obtaining for each region a number of diffraction patterns greater than 200000. The measurements were carried out continuously for several days in order to acquire all the necessary data, after the absence of surface contamination was determined by normal SEM imaging. Because indexing the diffraction pattern at each location gives a unique measure of the three-dimensional crystallographic orientation at that point, a large amount of information is obtained from this kind of measurement, both on the local and macroscopic structure of the sample's surface layer. Before starting diffraction pattern acquisition, observation of the sample's morphology was conducted in the same microscope. SEM micrographs of the sample's surface are reported in Figure 4.7. Figure 4.7 (a) was acquired with the sample tilted at an angle of 70° and a magnification of 5 Kx. Many particles are visible on the surface, but the film underneath looks very dense and smooth. Figure 4.7 (b) is a lower magnification micrograph obtained with a sample tilt of 0° . The elongated particles oriented at 45° with respect to the substrate edge and

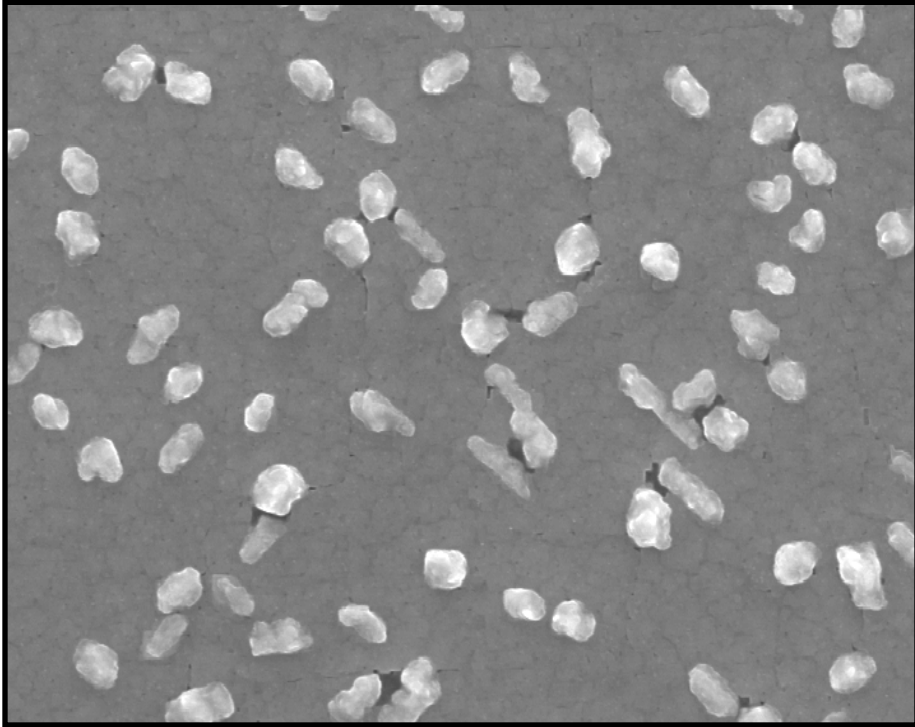
perpendicularly to each other are a-axis oriented grains; these grains sometimes are also observed in NdBCO films on single-crystal. Figure 4.7 (c) shows a higher magnification of a region in Fig. 4.7 (b). Besides the a-axis grains, some Ba-Cu-O particles (similar to those revealed on film deposited on single crystal) are clearly visible on the surface. The film looked very dense and compact, and pin-holes were completely absent. High magnification micrographs [Fig.4.7 (d) and (e)]



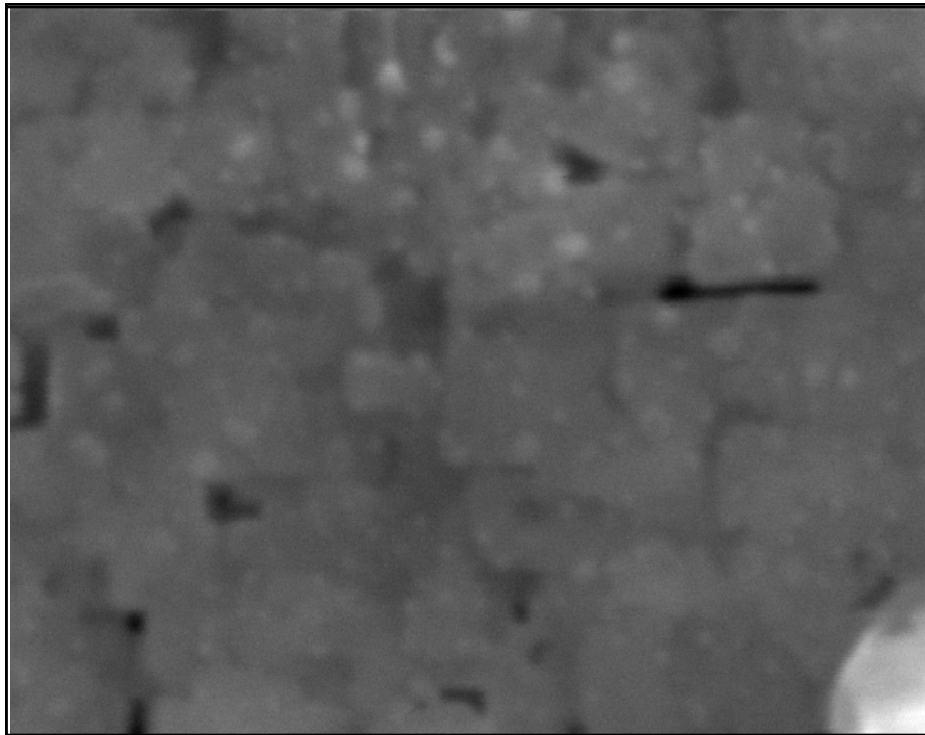
(a)



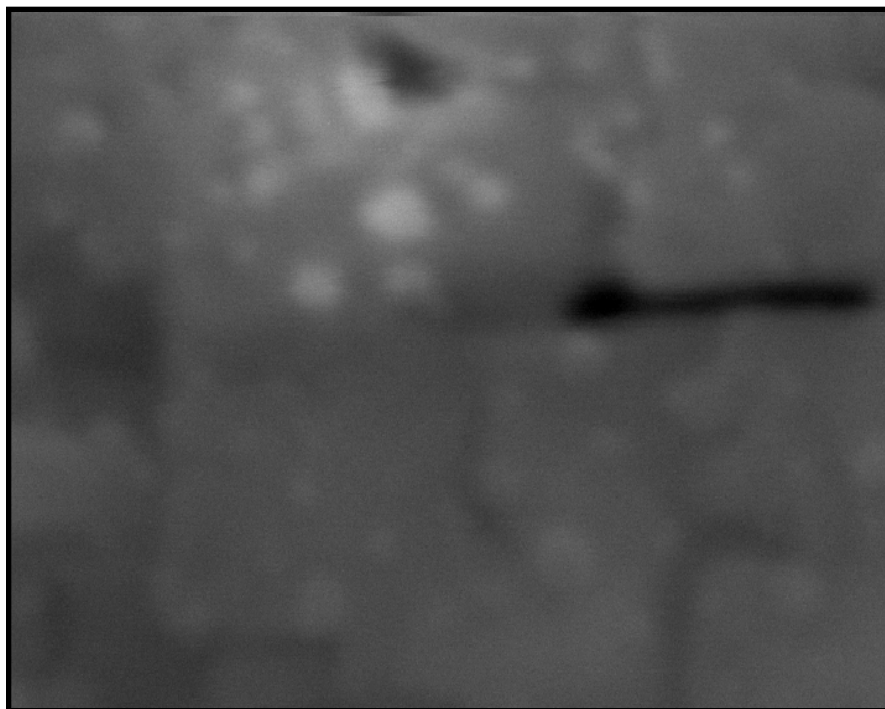
(b)



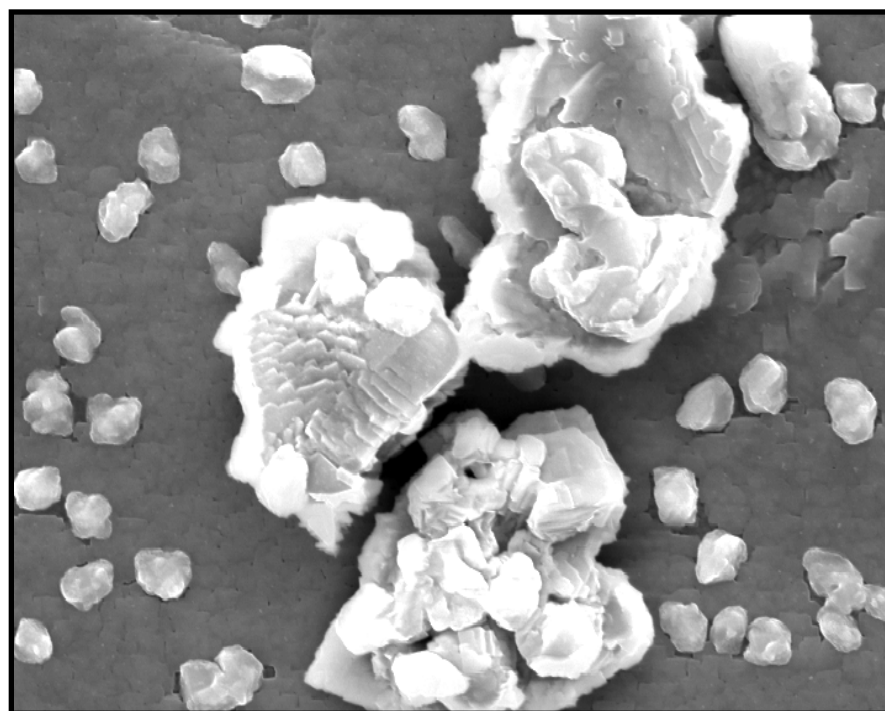
(c)



(d)



(e)



(f)

Fig.4.7. SEM micrographs of sample la062498Ni1 of different magnifications: (a), 5 Kx, $\phi = 70^\circ$; (b), 1 Kx; (c), 5 Kx; (d), 50 Kx; (e), 100 Kx; (f), 5 Kx.

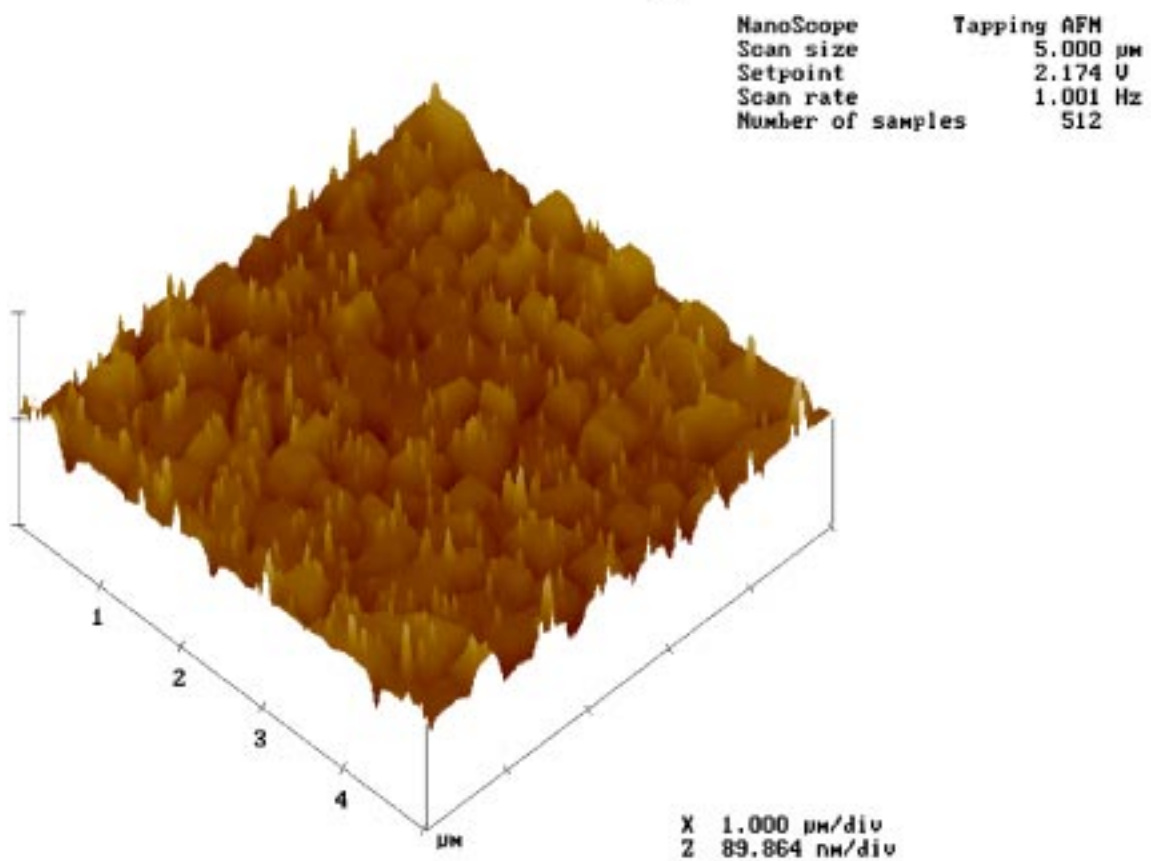
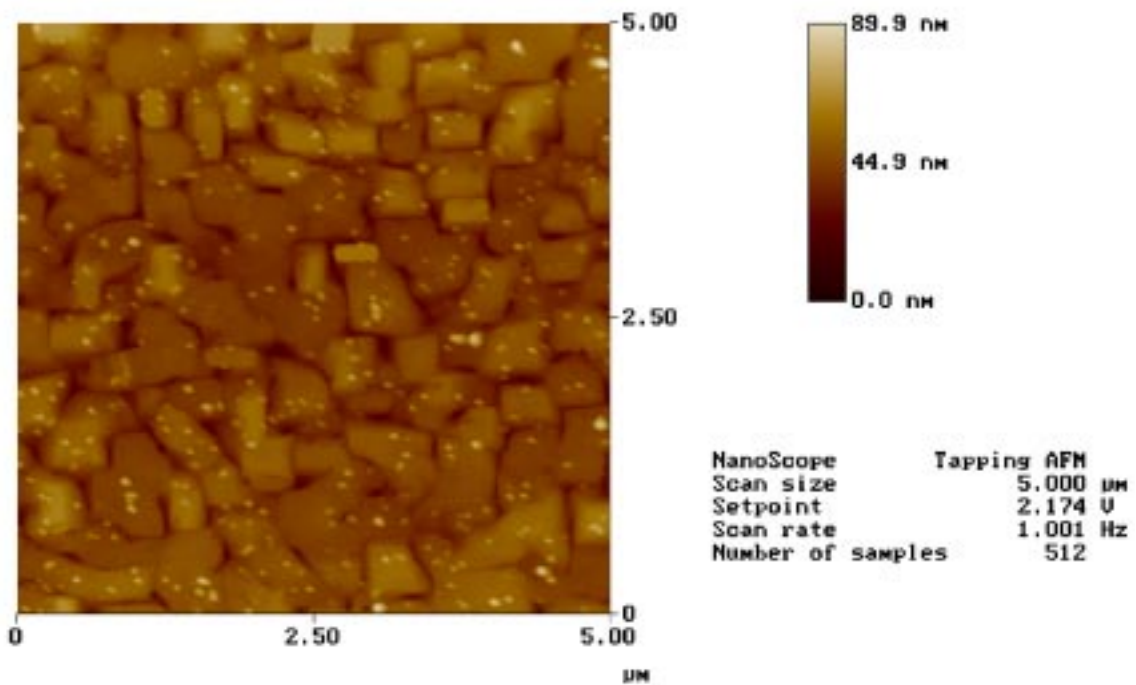


Fig. 4.8. *Top view and perspective view of the surface of a high T_C and J_C NdBCO film on $LaAlO_3$ acquired by AFM.*

revealed the presence of small, finely-dispersed precipitates. These small clusters were also observed sometimes in films deposited on single crystal. For comparison, an AFM image of a high T_C NdBCO film on $LaAlO_3$ is reported in Figure 4.8, showing a morphology very similar to that observed in the NdBCO films on RABiTS. In particular, the particles observed here are characterized by a lighter color because of their higher height with respect to the rest of the film. However, an understanding of the nature of these precipitates will have to wait transmission electron microscopy (TEM) analysis. Another relevant feature observed in sample la062498Ni1 is the presence of some YSZ particles of large dimensions ($\sim 5\mu\text{m}$) on top of the surface [Fig. 4.7 (f)]. These particles originated during the YSZ layer growth and the NdBCO film developed around them.

Fig. 4.9 (a) represents an orientation image micrograph of sample la062498Ni1. This image is not an SEM micrograph, but is the result of the electron diffraction patterns acquired by using a technique known as backscatter Kikuchi diffraction (BKD). Each point composing the figure is characterized by a different shade of gray according to the quality and intensity of the diffraction pattern at that point. Grain boundaries, as well as other crystallographic defects or particles on the surface, show a poor diffraction pattern and, consequently, these regions appear as darker points on the orientation map. It can be noticed that grain boundaries in the Ni substrate are transferred through the buffer layers to the superconductor structure, showing on the orientation map as darker lines. Black spots originating from the film's particles are also clearly visible. Electron diffraction patterns were acquired on a hexagonal grid with a spacing of $0.5\ \mu\text{m}$. The total number of patterns obtained in the region of nearly $0.5 \times 1\ \text{mm}$ reported in Figure 4.9 was 231868. Indexing the pattern at each location gave a unique measure of the

orientation at that point. In order to calculate the misorientation angle for each grain boundary, a hypothetical hexagonal lattice with a grain size of $0.5 \mu\text{m}$ was superimposed at each point from which a pattern was obtained. Thus, by processing the data, it is possible to calculate the grain boundary misorientation angles for all the resulting boundaries. In this way orientation maps are generated showing misorientation angle values at each grain boundary and the regions percolatively connected within a certain angle. Figure 4.9 (b) shows a regeneration of Figure 4.9 (a) with the following grain boundaries criteria: green boundaries have misorientation angles greater than 1° and less than 5° ; yellow boundaries have misorientation angles greater than 5° and less than 10° ; and red boundaries have misorientations greater than 10° . Figure 4.10 visualizes the percolation of a current flow. In fact, Figures 4.10 (a), (b), (c), (d), and (e) have been colored according to the criterion that a single color represents a contiguous or percolative region of orientation less than 1° , 2° , 3° , 4° , and 5° , respectively. As shown in Figure 4.10 (c), the NdBCO sample analyzed is well-connected by boundaries less than 3° , and thus exhibits an excellent in-plane orientation. The grain boundary misorientations get even smaller if we focus on a smaller region of the sample, such as that depicted in Figure 4.11 (a). This figure is the orientation image micrograph obtained from a region of $0.12 \times 0.2 \text{ mm}$ in size. Such a region is percolatively connected within only 1° , as shown in Figure 4.11 (b). A representation of the same region using criteria of percolation within 2° , 3° , and 4° is reported in Figure 4.12 (a), (b), and (c). Figure 4.12 (d) is a superimposition of Figure 4.12 (c) and the grain boundaries lines, with the colors green, yellow, and red having the same meaning as in Figure 4.9 (b).

The totality of the diffraction patterns acquired provides a complete representation of the three-dimensional crystallographic structure of the sample and contains all the information obtainable from the pole figures relative to all the

crystal poles. In fact, the diffraction patterns collected can be used to generate the pole figure for any one of the crystal planes families, providing all possible

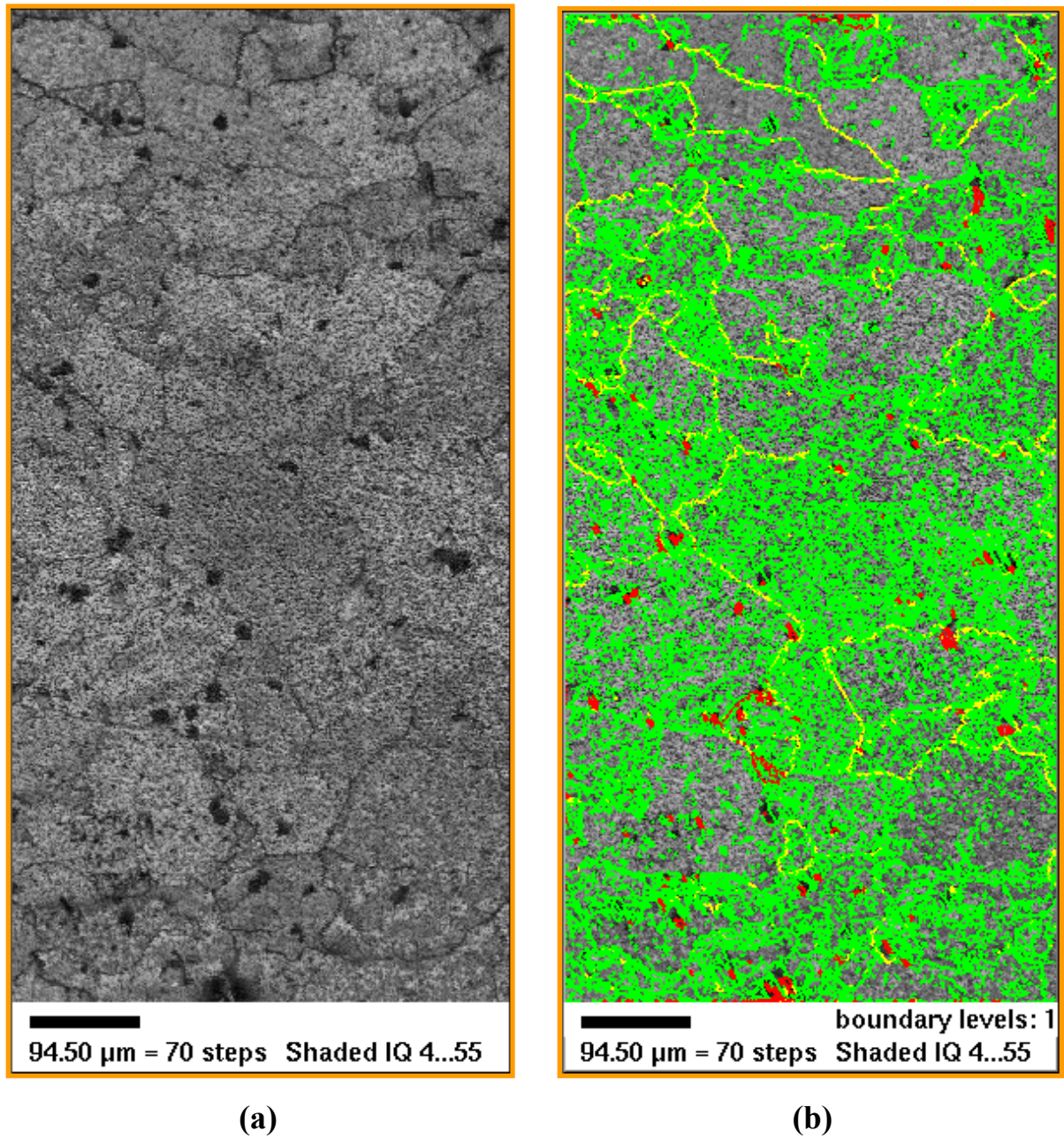
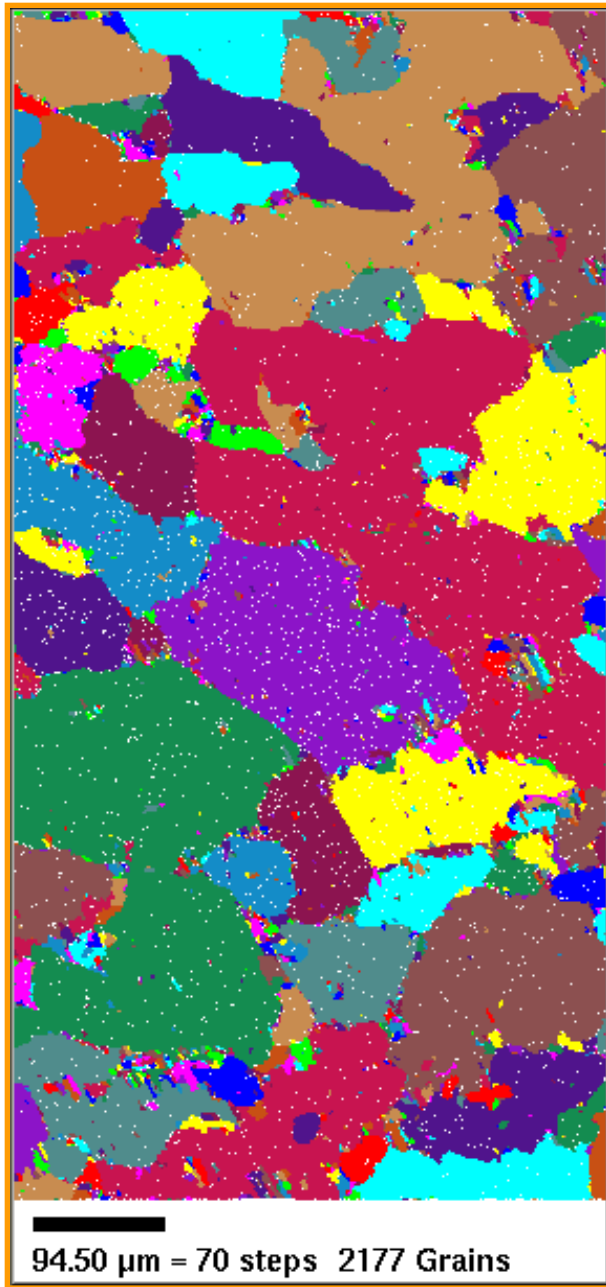
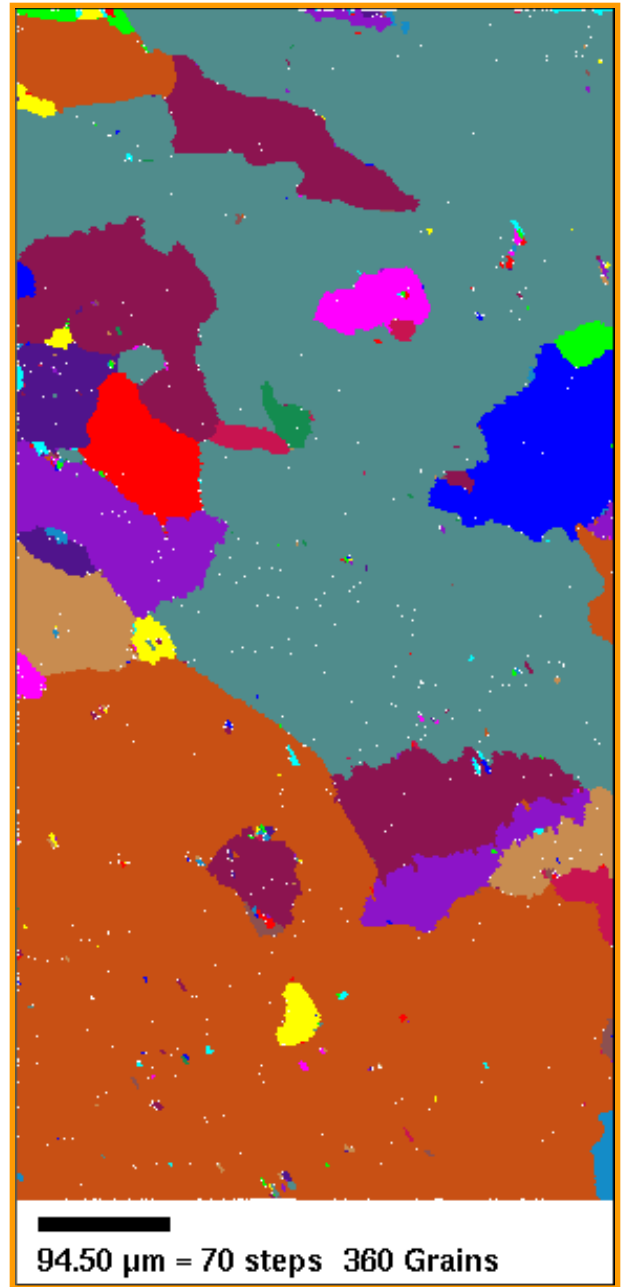


Fig. 4.9. Orientation image micrographs from a macroscopic region of sample la062498Ni1, (a). In figure (b), different colors indicate different grain boundary misorientation angles: between 1° and 5° , green; between 5° and 10° , yellow; and greater than 10° , red.



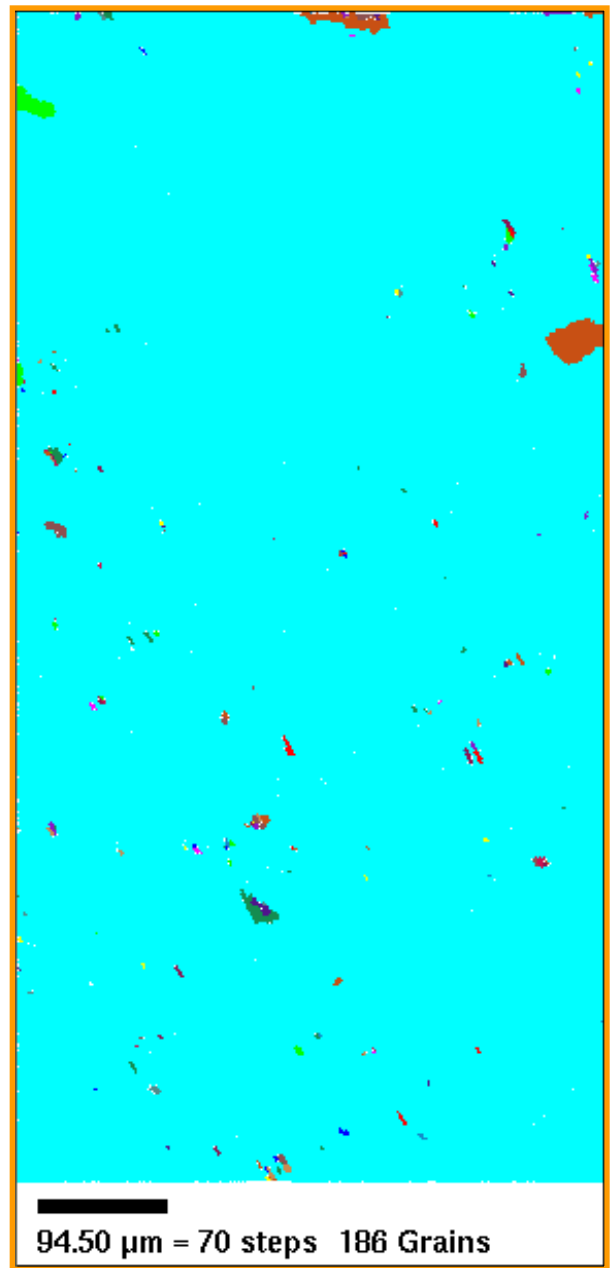
(a)



(b)



(c)



(d)

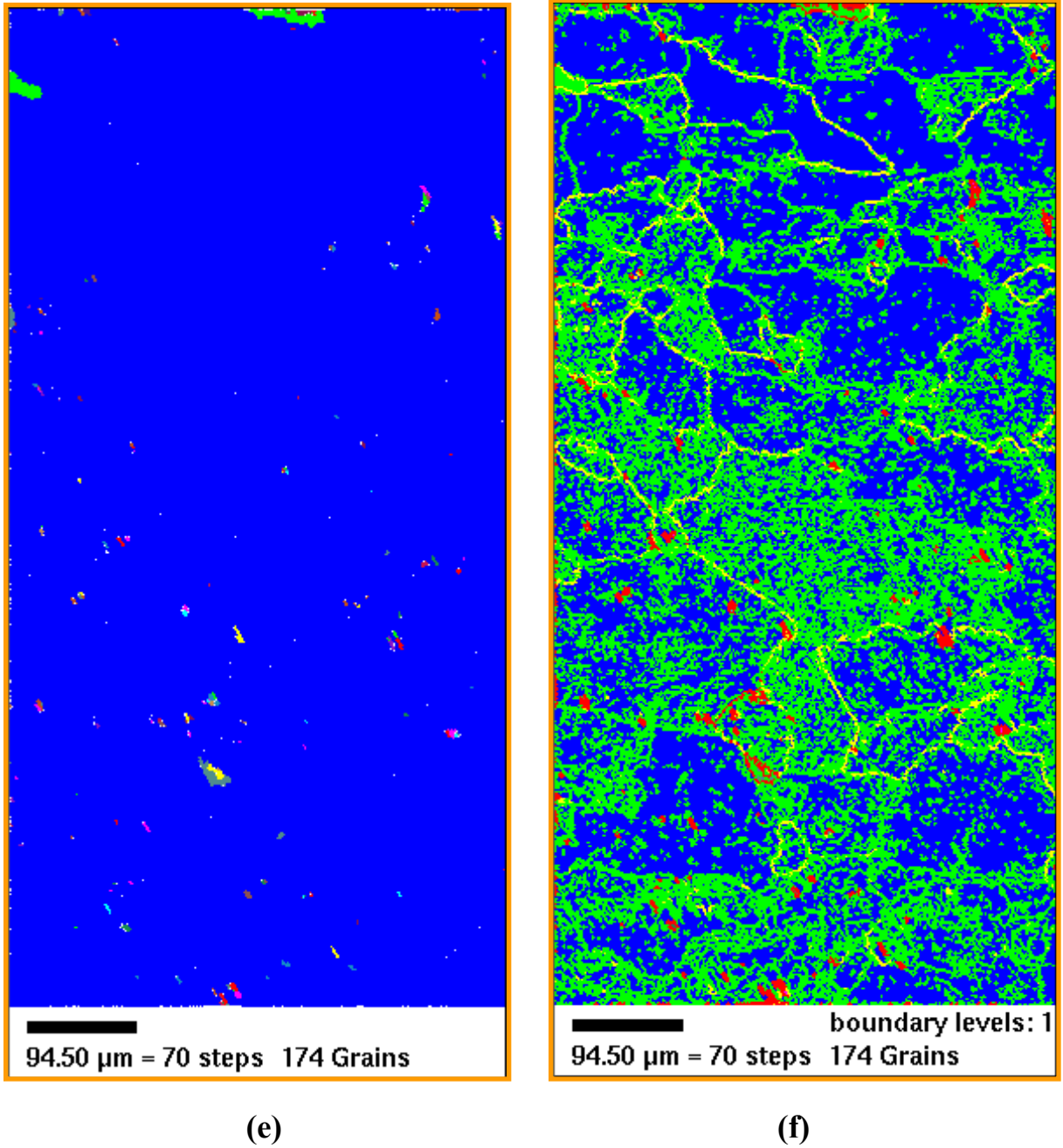
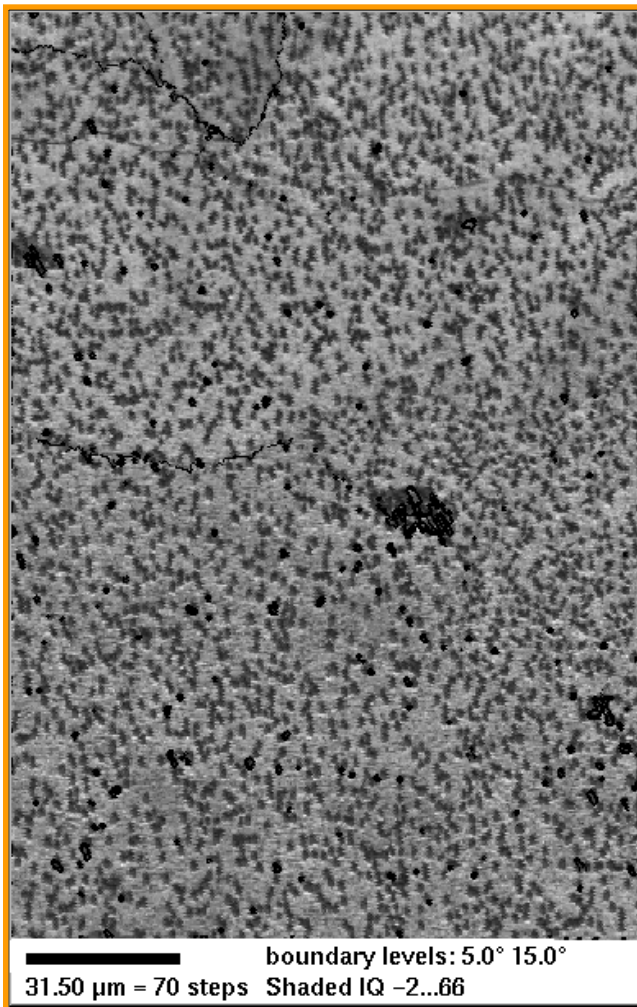
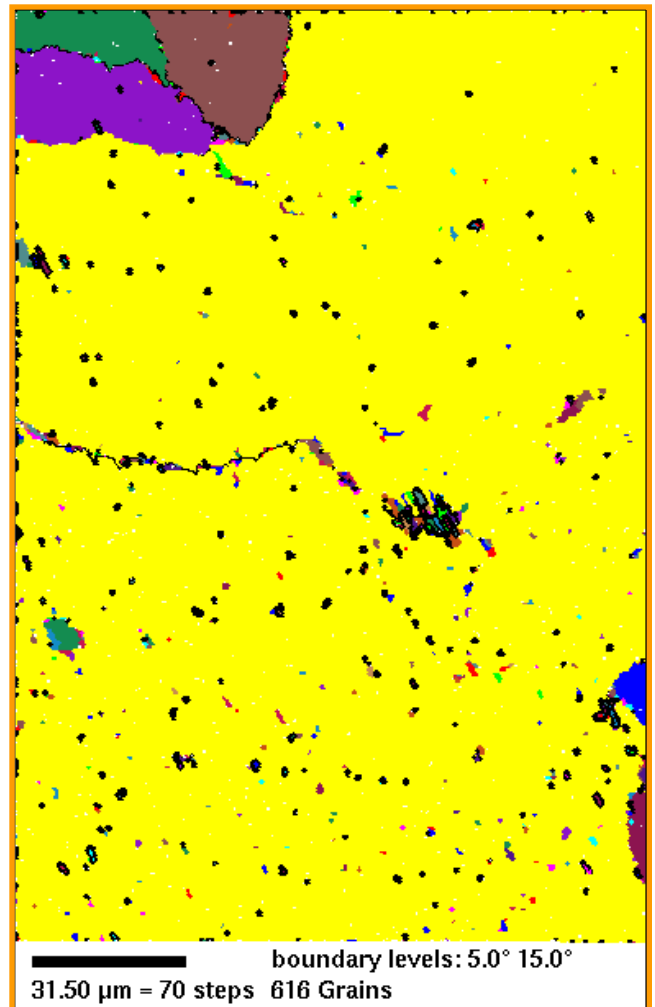


Fig. 4.10. Orientation image micrographs shown in Fig. 4.9 colored with the criterion that a given color represent a percolative region within 1° (a), 2° (b), 3° (c), 4° (d), 5° (e). Figure f is a superimposition of (e) and Fig.4.9 (b).

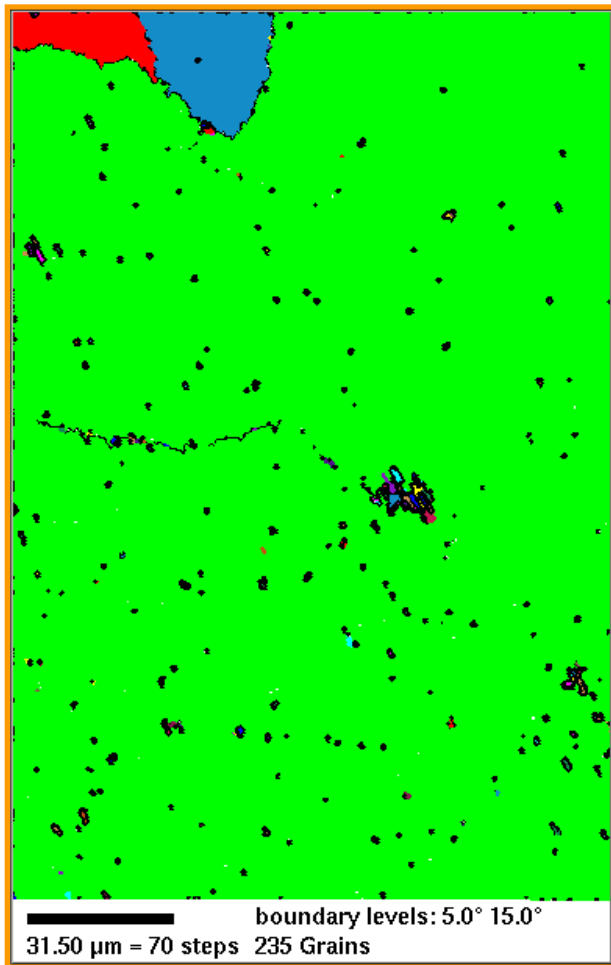


(a)

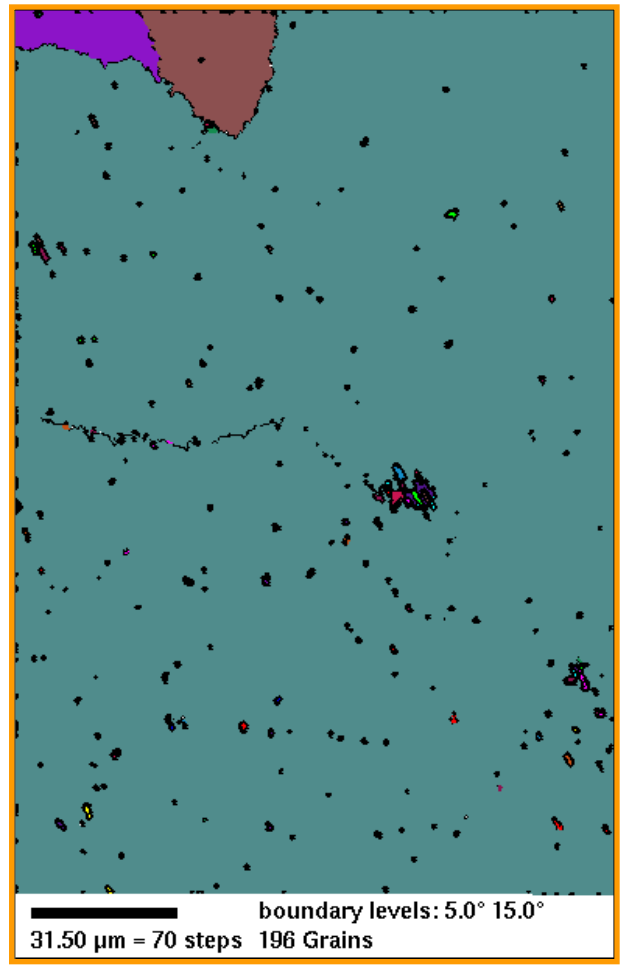


(b)

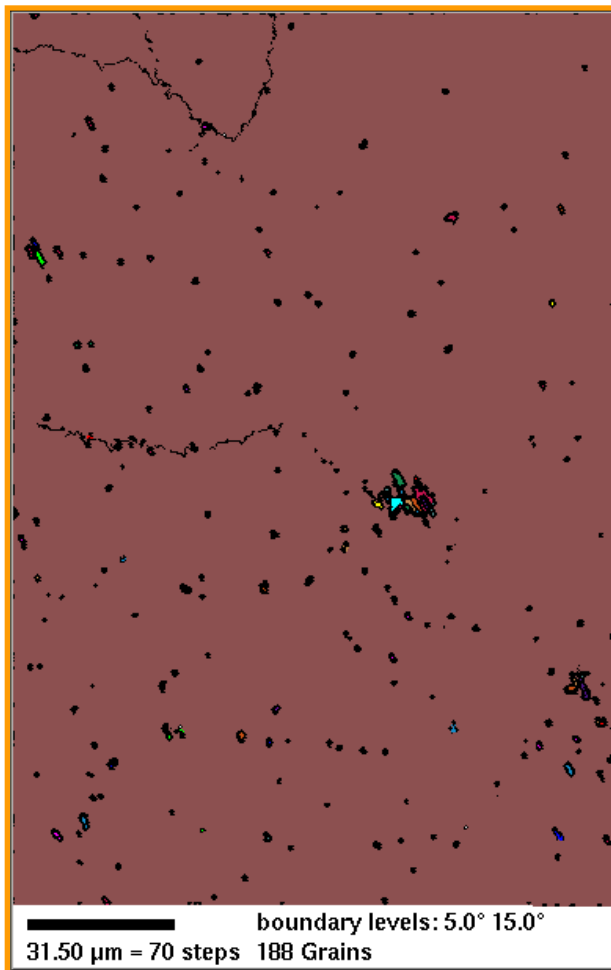
Fig.4.11. Orientation image micrograph obtained from 142250 diffraction patterns of a macroscopic region of sample la062498Ni1 (a). The same orientation image micrograph colored with the criterion that a given color represents a percolative region within 1° (b).



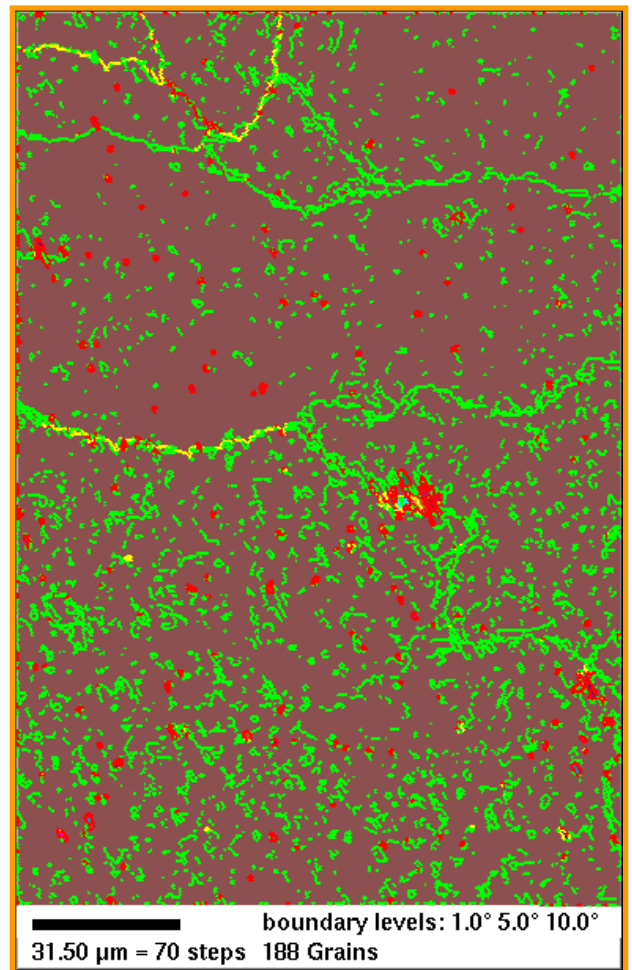
(a)



(b)



(c)



(d)

Fig. 4.12. Orientation image shown in Fig. 4.11 colored with the criterion that a given color represents a percolative region within 2° (a), 3° (b), 4° (c). (d) the grain boundary lines are superimposed to figure (c), with the usual color code: green for misorientation angles between 1° and 5° , yellow for misorientation angles between 5° and 10° , and red for misorientation angle greater than 10° .

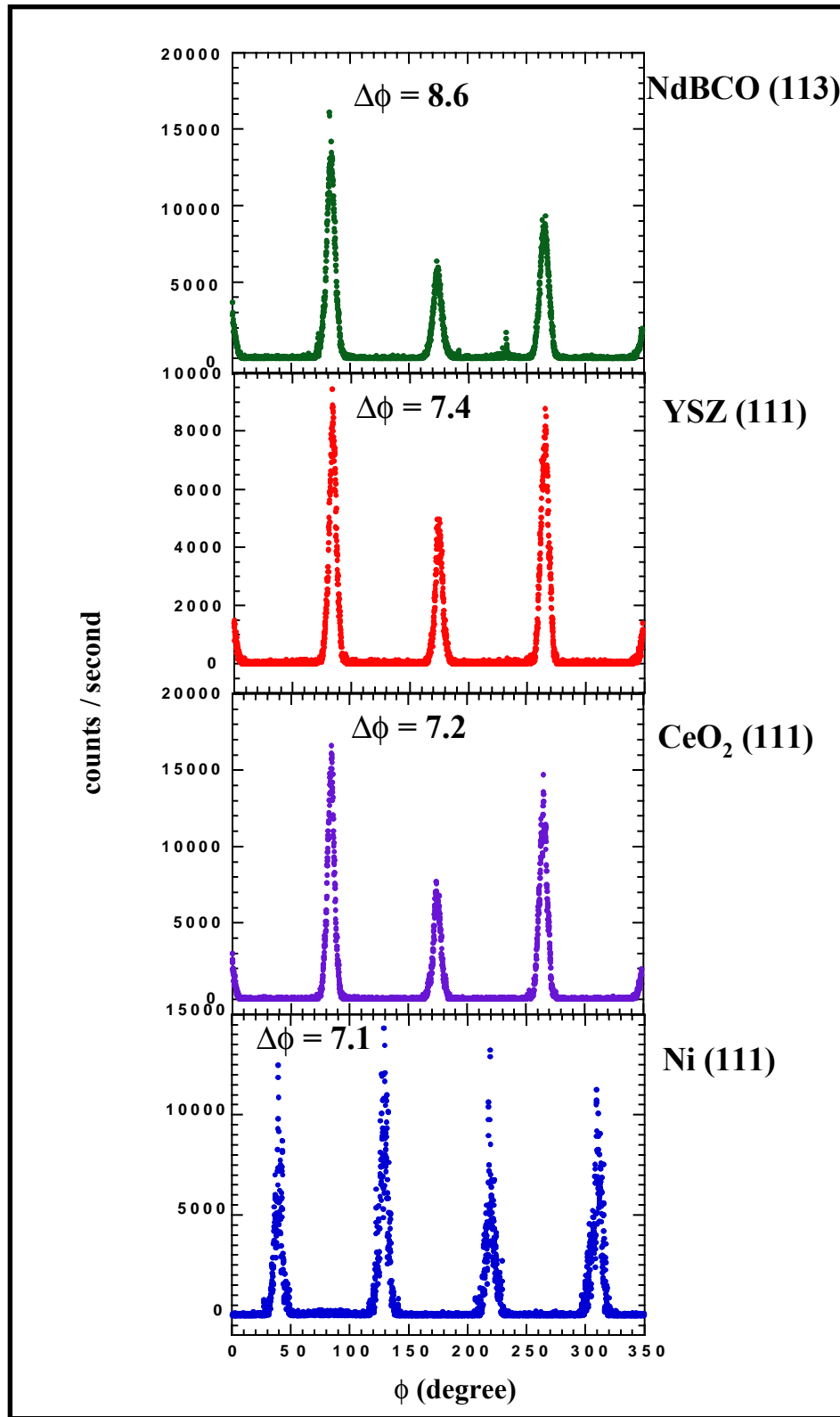


Fig. 4.13. X-ray ϕ -scans showing the in-plane texture of the rolled and annealed Ni substrate, the CeO₂ and YSZ buffer layers, and the NdBCO film in sample la082498Ni1.

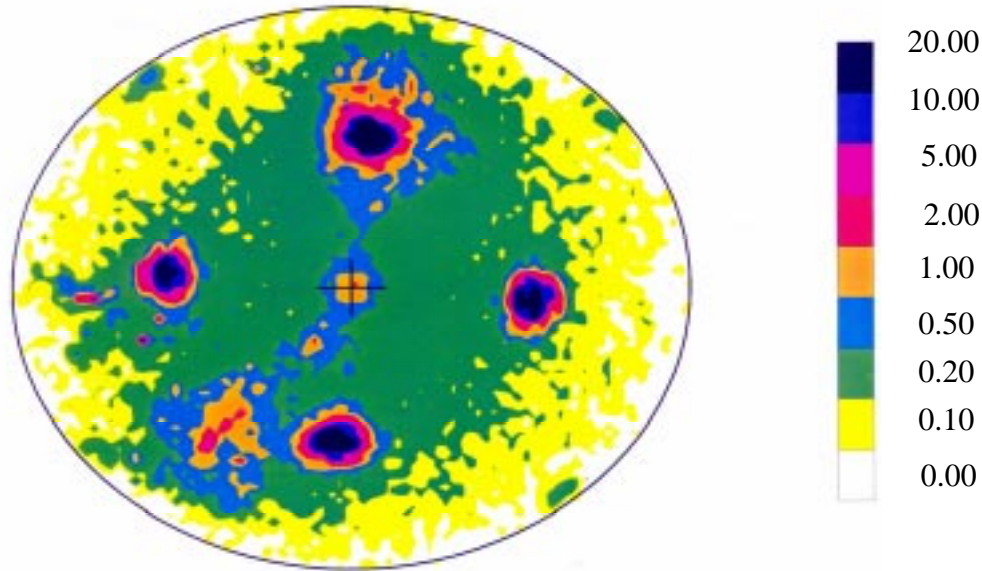


Fig. 4.14. Pole figure for the NdBCO (113) reflection. The color scale is a measure of the intensity of the patterns

information about the macroscopic three-dimensional orientation of the sample. The pole figures obtained by electron diffraction are analogous to the pole figures obtained by X-ray diffraction scans with the sample rotating in turn around all three Euler angles (ϕ , θ , and χ). The only difference is that, during backscattering electron measurement, diffraction data are acquired simultaneously for all the crystal poles, and only for a very thin surface layer (~ 20 nm). X-ray pole figures, instead, provide the orientation of all the buffer layers, the superconducting layer, and the Ni substrate. Consequently, in order to obtain information on the orientation of all the sample's layers, an X-ray characterization of sample la062498Ni1 was performed. The in-plane crystallographic alignment of the epitaxial NdBCO/YSZ/CeO₂/Ni structure was determined by ϕ -scans through the NdBCO (113), YSZ (111), CeO₂ (111), and Ni (111) planes. The out-of-plane

texture was determined by the XRD rocking curves (θ -scans) through the following peaks: NdBCO (006), YSZ (200), CeO₂ (200), and Ni (200). For each peak, two rocking curves were recorded by tilting the sample in the rolling direction, and in the direction perpendicular to this (about the rolling direction). The data for the (113) pole figure of the NdBCO layer also were collected.

A collection of the ϕ -scans for Ni (111), CeO₂ (111), YSZ (111), and NdBCO (113) for the peaks is reported in Figure 4.13. The FWHM values are 7.13, 7.23, 7.42, and 8.64 respectively, showing a very good alignment. It can be noticed that the cerium oxide grows with a 45° axis rotation with respect to the nickel substrate. The YSZ film, in turn, grows with the <100> axis oriented along the CeO₂ <100> axis. The in-plane texture of the NdBCO film is reported in detail in Figure 4.14, where we show the NdBCO (113) pole figure, which is a representations of a collection of ϕ -scans, each acquired at a different χ -angle. The NdBCO axes are 45° rotated with respect to the YSZ axes and aligned with the Ni *a* and *b* axes. However, because the NdBCO (113) reflection is, in turn, 45° rotated with respect to the YSZ (111) reflection, the ϕ -scan and the pole figure of NdBCO appear 45° rotated with respect to those of the Ni substrate.

The peak observed in the center of the pole figure is due to X-ray fluorescence, while the feature present at one side of the figure that does not show a four-fold symmetry is only an artefact of the equipment.

A collection of rocking curves for the peaks Ni (200), CeO₂ (200), YSZ (200), and NdBCO (006), in and about the rolling direction is reported in Figures 4.15 and 4.16. The alignment of the *c*-axis is always better in the rolling direction of the Ni substrate,, where we find FWHM values of 7.72°, 6.65°, 6.63°, and 6.44° for the Ni, CeO₂, YSZ, and NdBCO peaks respectively.

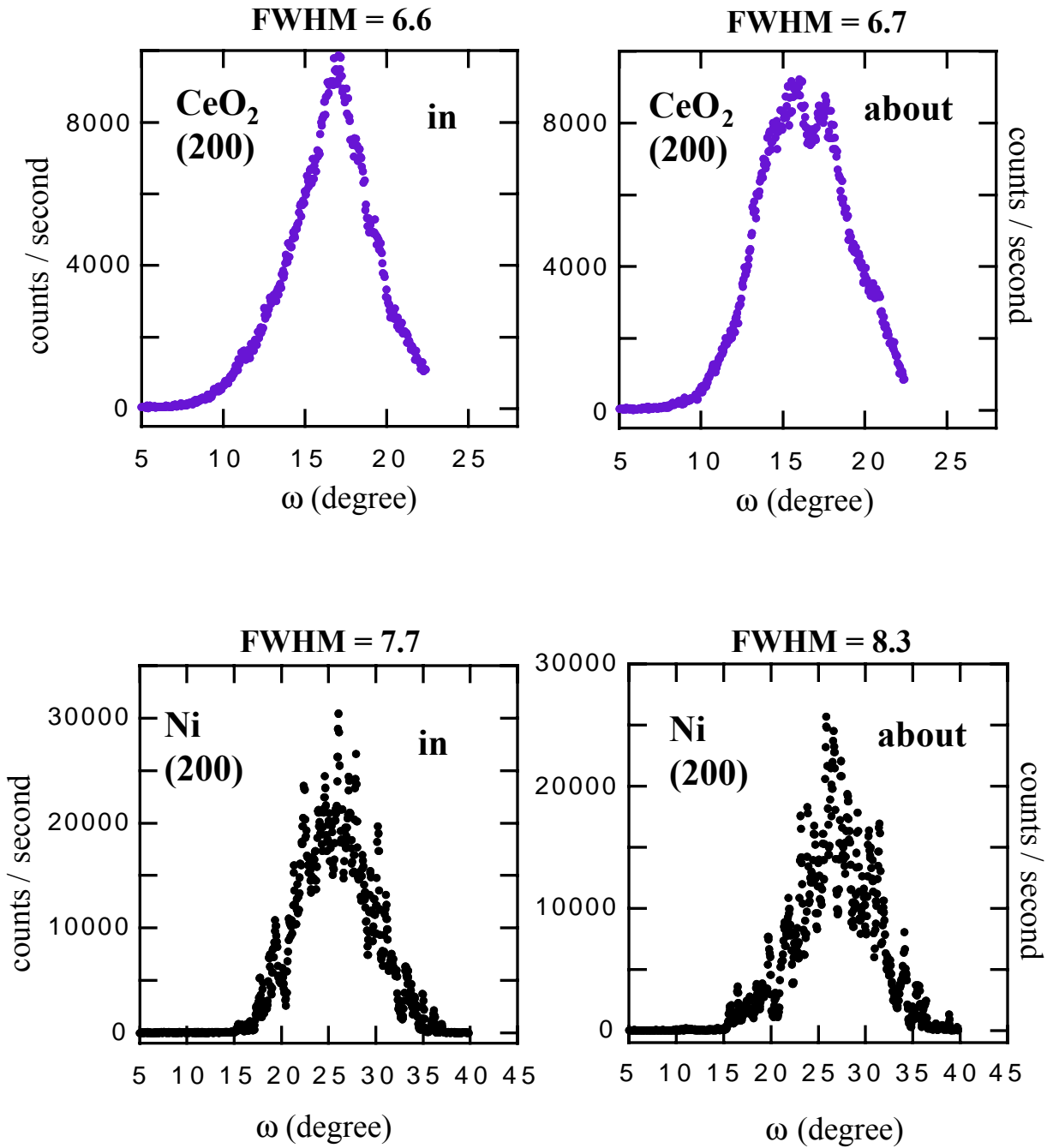


Fig. 4.15. Rocking curves for the Ni substrate and the CeO₂ buffer-layer in the direction of rolling (in), and in the direction perpendicular to this (about).

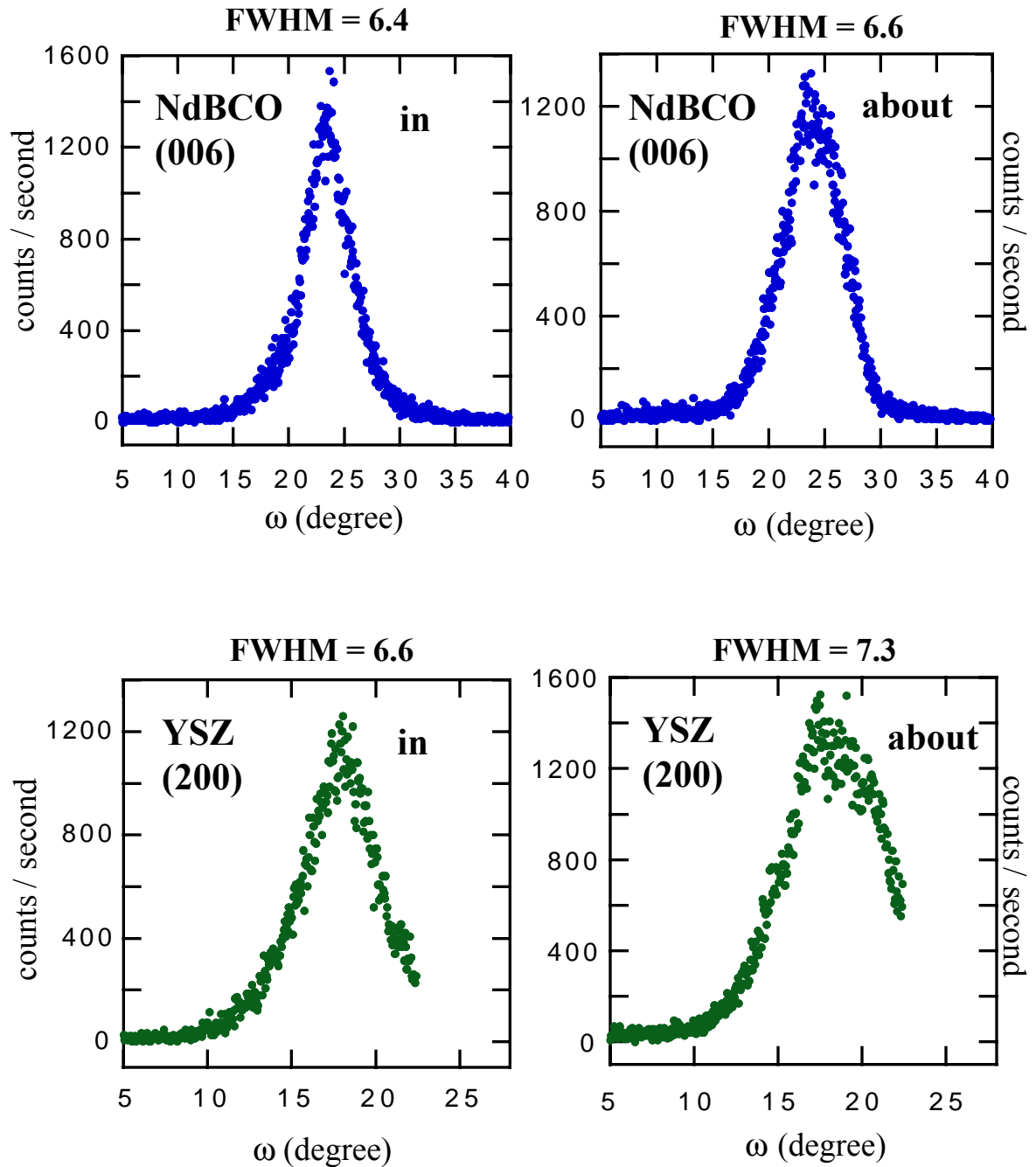


Fig. 4.16. Rocking curves for YSZ (002) and NdBCO(006) in the direction “in and “about”.

Transport critical current measurements and field dependence

The critical current J_C was evaluated through direct transport measurements. The J_C dependence on magnetic field was measured with the field varying from 0 T to the irreversibility field, which is measured as the lower-limit field value at which the current flowing through the superconductor switches from a power function of the voltage measured to a linear function and flux flow regime takes place. In all NdBCO samples for which the J_C field dependence was measured, the irreversibility field was higher than 6 T, indicating the presence of strong flux pinning. J_C values of 200 KA/cm² measured at 77 K and zero field were obtained for NdBCO films on RABiTS. This value is comparable with the J_C values measured for the YBCO films on RABiTS grown for this project, but is lower than the optimal values (ranging around 1 MA/cm²) obtained at ORNL for YBCO/RABiTS using the same technique.

Fabrication of high quality RABiTS substrate is not a trivial task, and phenomena such as the presence of micro-cracks in the buffer-layer, recrystallization of the Ni substrate during growth, interdiffusion between the substrate and buffer-layer, Ni oxidation, or other type of structural defects, can often occur during deposition and more or less seriously affect superconducting layer growth. The quality of the Ni substrate is another important parameter for a good final result. Consequently, more samples than those developed for this project need to be prepared to obtain a more precise estimate of the critical current carried by NdBCO films on RABiTS. The best YBCO films on RABiTS usually show a J_C value at H=0 lower than that measured for films on single crystal, but J_C decreases less rapidly with the magnetic field than it does in YBCO films on single crystal. Consequently, the two J_C versus H curves (relative to YBCO/RABiTS and YBCO/single crystal) often show a cross-over point, and, at high magnetic field (5-6 T), RABiTS

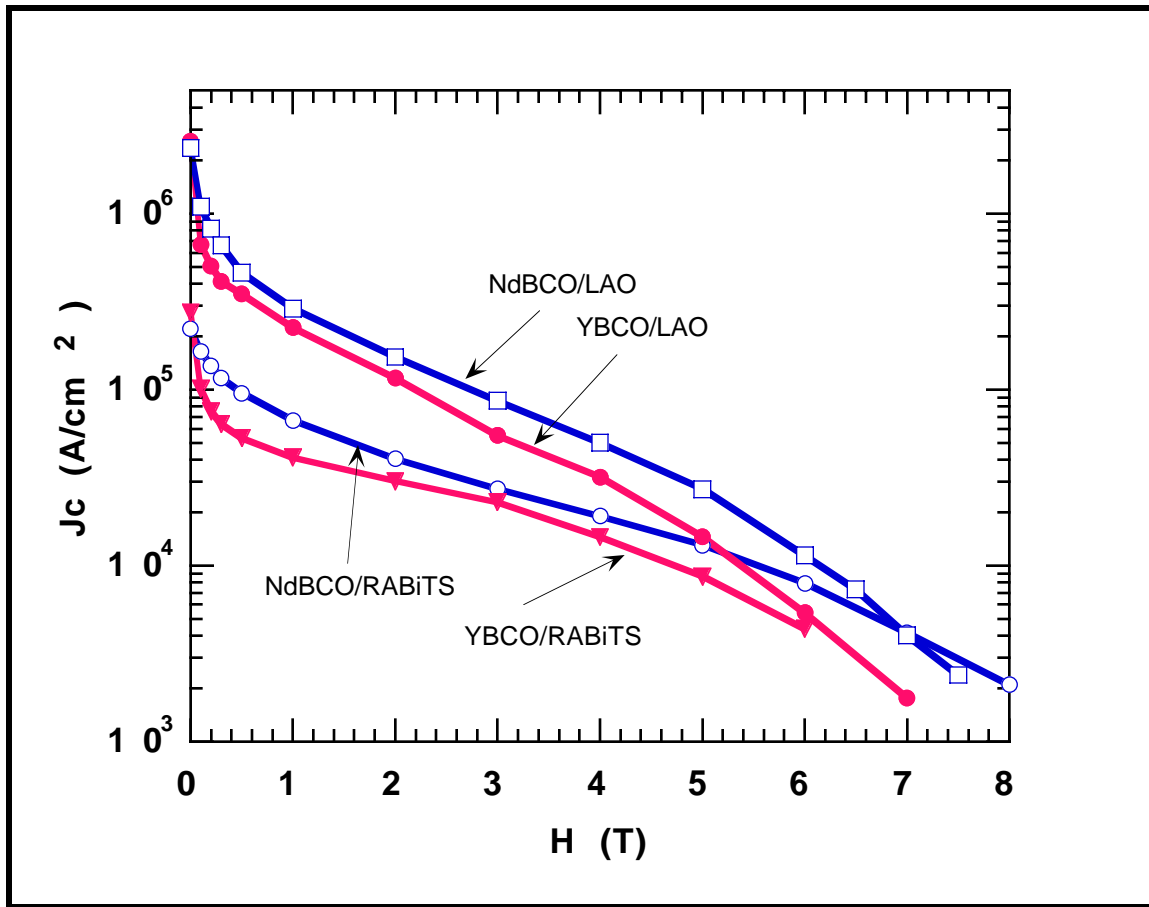


Fig. 4.4. J_c dependence on magnetic field at 77 K for NdBCO and YBCO films deposited on $LaAlO_3$ and RABiTS substrates.

samples exhibit higher J_c than those on single crystal. This behavior is indicative of the presence in RABiTS samples of a higher number of defects that act as strong pinning sites when a magnetic field is applied. As regards NdBCO samples on RABiTS, in spite of the not extremely high $J_c(H=0)$, we observed high J_c values in high magnetic field and a very high irreversibility field ($H_{irr} = 8$ T). These results are consistent with the observation of an increased number of pinning sites in RABiTS samples.

A comparison between various J_c versus H curves for NdBCO and YBCO on RABiTS and LaAlO₃ substrates is reported in Figure 4.4. As can be noticed, the best YBCO and NdBCO films obtained on LaAlO₃ show very similar $J_c(H)$ curves. Moreover, NdBCO films appear to carry a slightly higher current than YBCO films at high magnetic fields, and also show a higher irreversibility field than YBCO. The NdBCO film on RABiTS shows a J_c at $H = 6$ T equal to the value usually measured for YBCO films on single crystal, and exhibits a very high J_c in the interval (6-8 T). We also observed that J_c in NdBCO/RABiTS samples exhibits the same behavior with magnetic field as that reported for NdBCO on single crystal, and no "peak effect" was revealed.

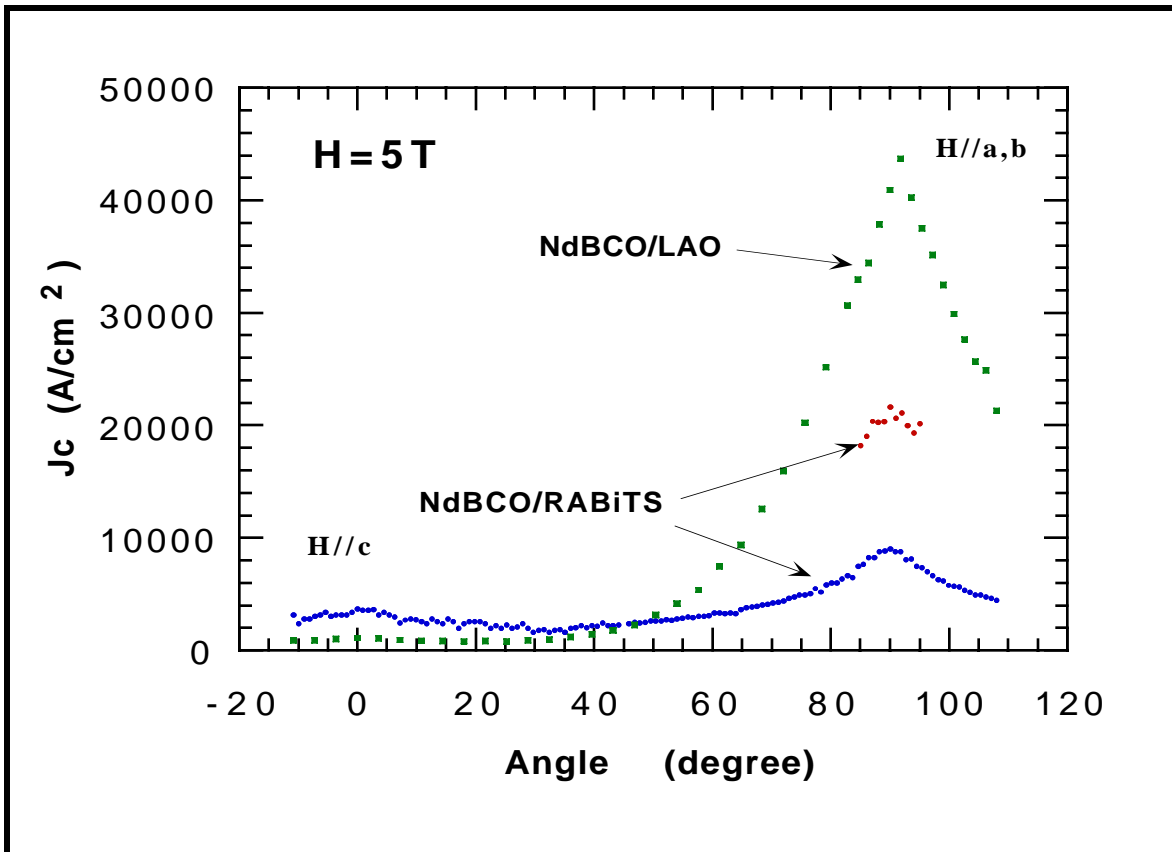


Fig. 4.5. Angular dependence of J_c measured at $H = 5$ T for NdBCO films on RABiTS and LaAlO₃ (LAO) substrates.

Figure 4.5 shows the J_c dependence on the angle between the magnetic field and the film's c-axis, measured for samples other than those reported in Fig. 4.4, and for an applied magnetic field of 5 T. We observe the reported enhancement in J_c at high magnetic field for films on RABiTS compared to films on single crystal in the region near to $H//c$. However, such enhancement is accompanied by a suppression in the critical current in the region near to $H//a,b$. Such behavior has also been reported for YBCO films on RABiTS substrates and is believed to originate from the presence of some sort of strong-pinning extended defects in RABiTS samples that would extend upward through the film, enhancing vortices pinning in the configuration with $H//c$.

In conclusion, the NdBCO film on RABiTS considered above showed an optimal structure: dense, characterized by well-connected grains, and with an excellent epitaxy. Moreover, we did not observe any trace of microcracks that could cause a suppression of J_c . Such a structure is revealed only by the best YBCO films on RABiTS, that consequently exhibit very high J_c ($> 1\text{MA}/\text{cm}^2$), and is not consistent with a J_c of only $200\text{KA}/\text{cm}^2$ measured for our sample. The reasons for a J_c lower than that observed in NdBCO films on single crystal substrates, deposited in the same conditions, is thus attributable to other causes. Since Ni substrates and insulating substrates like LaAlO_3 or SrTiO_3 have a very different thermal conductivity, it is possible that for a given heater temperature, during film deposition, different substrates actually have different temperatures. According to the study performed on NdBCO films deposited on LaAlO_3 , changing the substrate temperature for film growth by $20\text{ }^\circ\text{C}$ leads to a small difference in the film's T_c , but a considerable suppression of J_c (almost one order-of-magnitude). Consequently, in a situation in which all the other deposition parameters are unchanged, substrate temperature difference is the most probable cause of the

lower J_c observed for the samples on RABiTS. This hypothesis constitutes the starting point for a future investigation to address the processing of NdBCO films on RABiTS with very high J_c . At present, the result of an irreversibility field of 8 T for a sample showing only a moderate J_c at $H=0$, in addition to a measured T_{c0} of 93 K, is very interesting and encouraging for further research on NdBCO.

CONCLUSIONS

The first aspect of the research presented here is a systematic investigation of the superconducting properties of NdBCO films. Because of the existence of the solid solution $\text{Nd}_{1+x}\text{Ba}_{2-x}\text{Cu}_3\text{O}_y$, NdBCO film synthesis was very sensitive to small variations in all the deposition parameters and required a significant effort. The optimization of the superconducting transport properties of NdBCO films was obtained by growing a considerable number of samples (about 100) and studying the influence of numerous deposition and annealing parameters, including background pressure, substrate temperature, laser energy, laser-target distance, target composition, cooling paths, deposition rate, and duration and temperature of the heat treatments. Such a study involved measurements of samples' electrical and magnetic properties, composition, morphology, and crystal structure, by numerous techniques.

The effect of the oxygen partial pressure during film growth was analyzed by varying this pressure in a range of four orders-of-magnitude, for a substrate temperature (T_s) range of 730 °C to 800 °C. The experiment was motivated by results reported in the literature on bulk synthesis and considerations on the YBCO P-T phase diagram. On this basis it was hypothesized that the thermodynamic stability curve in the $P(\text{O}_2)$ -T phase-space for in-situ NdBCO film synthesis would be shifted towards reduced oxygen pressure values relative to the $\text{YBa}_2\text{Cu}_3\text{O}_{7-\delta}$ (YBCO) curve (Hammond and Bormann line). Consequently, deposition conditions appropriate for the growth of NdBCO films were expected to differ significantly from those successfully used for YBCO. The results obtained confirmed this hypothesis showing a clear dependence of films superconducting properties on the oxygen partial pressure during growth. A plot of the conditions [T_s , $P(\text{O}_2)$] for optimal film synthesis in the $\log[P(\text{O}_2)]-1/T$ phase-

space determined a line almost parallel to the corresponding Hammond and Bormann line for YBCO films, but shifted with respect to the Hammond and Bormann line by about two orders-of-magnitude. The optimization of NdBCO film growth resulted in the reproducible synthesis of samples with T_c 's of 93 K and J_c 's above 2 MA/cm².

The J_c dependence on magnetic field observed for NdBCO films was similar to that reported for YBCO films. However, a smaller reduction of J_c with increasing magnetic field, and a higher irreversibility field compared to YBCO were observed in the best NdBCO films grown. Neither stoichiometric NdBCO films nor films with presence of small amounts of Nd-Ba antisite defects showed the peak in the J_c dependence on magnetic field that has been observed in bulk samples. This behavior suggests that the critical current in epitaxial films is dominated by the density of growth-induced structural defects that act as pinning centers. These defects, such as dislocation and stacking faults originating from impurities and imperfections on the substrate surface, have a much higher density in epitaxial films than in bulk samples. Consequently, $J_c(H)$ in epitaxial films is typically two orders-of-magnitude higher than J_c in bulk samples, and a weaker field-activated pinning mechanism, if present, can be easily masked.

The work conducted on NdBCO film growth on single-crystal substrates was a precursor to a second aspect of this thesis that involved deposition of HTS films on metallic substrates. Rolled-assisted-biaxially-textured-substrates (RABiTS) were fabricated by depositing YSZ and CeO₂ buffer-layers on rolled and annealed Ni substrates by PLD. Subsequently, NdBCO and YBCO films were deposited on the RABiTS using the parameters for optimal film growth previously determined. The samples were characterized by electrical transport measurements, X-ray diffraction, scanning electron microscopy and backscattered electron diffraction. The in-plane and out-of-plane alignment of the NdBCO layer and the

YSZ/CeO₂/Ni architecture were evaluated by acquiring ϕ -scans and rocking curves for specific planes of the Ni, CeO₂, YSZ, and NdBCO layers. The results showed excellent epitaxy of the buffer-layers on the metal substrate and a very good in-plane and out-of-plane texture, with FWHM values of the ϕ -scans for the Ni(111), CeO₂(111), and YSZ(111) peaks of nearly 7°, and FWHM values for the rocking curves of the Ni(200), CeO₂(200), and YSZ(200) peaks of nearly 6.5°. The CeO₂ a,b axes were rotated 45° degrees with respect to the Ni axes, while the YSZ a, b axes were aligned with the CeO₂ in-plane axes. The NdBCO layer showed very good epitaxy with the in-plane axes rotated 45° with respect to the YSZ axes. A rocking curve of the NdBCO (006) peak and a ϕ -scan of the NdBCO(113) peak showed FWHM values of 6.4° and 8.6° respectively.

X-ray diffraction data give information on the macroscopic average of the orientations of the sample's grains. Consequently, from X-ray FWHM data it is not possible to extract a realistic estimate of J_c . More precisely, assuming a value of 8.6° for the grain-boundary misorientation angles would correspond to a J_c much lower than that actually measured. In fact, the most important parameter for obtaining high J_c values (10⁶ A/cm²) is the local existence of small (< 5°) grain boundary misorientation angles between adjacent grains, and the consequent formation of a low-angle percolative path along the sample.

A study of the grain-boundary misorientation distribution was conducted by backscattered electron diffraction. The results obtained by acquiring and indexing a number of diffraction patterns close to 250000 for a macroscopic sample region with dimensions of 0.5 x 1 mm, showed that the sample was percolatively connected by misorientation angles lower than 3°. This value is particularly good and typically correspond to J_c values of about 1 MA/cm² in YBCO films on RABiTS. However, transport current measurements on the NdBCO/RABiTS samples gave a J_c of 200 KA/cm², while T_c was in the range of

92 to 93 K. The lower J_c with respect to the values measured for NdBCO films on LaAlO₃ can be explained by considering that, for a constant heater temperature, the actual Ni substrate temperature could differ significantly from the temperature of an insulating single-crystal substrate. Such a difference could produce a variation in the 123 stoichiometry of NdBCO, which is highly sensitive to small composition changes, and thus suppress J_c . In spite of the relatively low J_c value at 0 T ($T = 77$ K), J_c measurements in applied magnetic field showed a very high irreversibility field ($H_{irr} = 8$ T). This result, combined with the optimal texture and the high T_c , indicates that improving HTS wires performance by using NdBCO as a superconducting layer is possible, and that further optimization of the superconducting properties of NdBCO films on RABiTS substrates would be worthwhile.

I wish to thank Professor S. Pace and Dr. V. Boffa for their suggestions, and especially for the opportunity they gave me to conduct this research at ORNL.

I would like to thank all the co-workers and friends I met during my stay at the ENEA Laboratory in Frascati, for creating a particularly pleasant environment.

At Oak Ridge National laboratory I have had the privilege of working in a group of brilliant scientists. Among them I wish in particular to thank Dr. D. P. Norton, Dr. D. K. Christen, D. M. Kroeger, and Dr. R. Feenstra for their precious scientific advises and discussions. The contributions to the measurements of Dr. M. Paranthaman, Dr. A. Goyal, Dr. D. Verebelyi, and Dr. E. Specht are highly appreciated.

I also wish to tank greatly J. W. Saulsbury for his moral support and continuous help with the English grammar.

References

- [I.1] T. P. Sheahen and A. M. Wolsky "Introduction to High-Temperature Superconductivity" Edited by T. P. Sheahen, Plenum Press (1994) ch 16.
- [I.2] D. Dimos, P. Chaudhari, J. Mannhart and F. K. LeGoues, Phys. Rev. Lett. 61 (1988) 219; D. Dimos, P. Chaudhari, and J. Mannhart, Phys. Rev. B 41 (1990) 4038.
- [I.3] K. Salama, V. Selvamanickam, and D. F. Lee, Bulk Materials: Processing and properties of High T_c superconductors, ed. Jin. S (Singapore: World Scientific, 1993) p 155.
- [I.4] I. Monot, K. Verbist, M. Hervieu, P. Laffez, M. P. Delamare, J. Wang, G. Desgardin, G. Van Tendeloo, Physica C 274 (1997) 253.
- [I.5] J. Wang, I. Monot, X. Chaud, A. Erraud, S. Marinel, J. Provost, G. Desgardin, Physica C 304 (1998) 191.
- [1] W. Wong-Ng, B. Paretzkin, and E. R. Fuller Jr., Adv. X-ray Analysis 33 (1990) 453.
- [2] T. B. Lindemer, E. D. Specht, P. M. Martin, and M. L. Flitcroft, Physica C 219 (1994) 145.
- [3] K. Osamura and W. Zhang, Z. Metallkd. 84 (1993) 522.
- [4] K. Takita, H. Akinaga, H. Katoh, H. Asano and K. Masuda, Jpn. J. Appl. Phys. 27 (1988) L67.
- [5] K. Takita, H. Katoh, H. Akinaga, M. Nishino, T. Ishigaki, and H. Asano, Jpn. J. Appl. Phys. 27 (1988) L57.
- [6] K. Takita, H. Akinaga, T. Ohshima, Y. Takeda, and M. Takano, Physica C 191 (1992) 509.
- [7] K. Takita, H. Akinaga, H. Katoh, and K. Masuda, Jpn. J. Appl. 27 (1988) L1676.

- [8] M. W. Shafer, T. Penney, B. L. Olson, R. L. Greene, and R. H. Koch, *Phys. Rev. B* 39 (1989) 2914.
- [9] M. Gupta and R. P. Gupta, *Physica C* 185-189 (1991) 321.
- [10] R. Nagarajan, R. Vijayaraghavan, L. Ganapathi, R. A. Mohan Ram, and C. N. R. Rao, *Physica C* 158 (1989) 453.
- [11] B. W. Veal and A. Paulikas, *Physica C* 184 (1991) 321.
- [12] M. J. Kramer, S. I. Yoo, R. W. McCallum, W. B. Yelon, H. Xie, and P. Allenspach, *Physica C* 219 (1994) 145.
- [13] R. Feenstra, D. P. Norton, J. D. Budai, D. K. Christen, D. H. Lowndes, V. C. Matijasevic, C.-B. Eom, T. H. Geballe, E. S. Hellman, and E. H. Hartford, "Layered Superconductors: Fabrication, Properties, and Applications", edited by D. T. Shaw, C. C. Tsuei, T. R. Schneider, and Y. Shiohara (Material Research Society Proceedings 275, Pittsburgh, PA 1992).
- [14] H. Shaked, B. W. Veal, J. Faber, Jr., R. L. Hitterman, V. Balachandran, G. Tomlins, H. Shi, L. Morss, and A. P. Paulikas, *Phys. Rev. B* 41 (1990) 4173.
- [15] B. W. Veal, A. P. Paulikas, J. W. Downey, H. Claus, K. Vandervoort, G. Tomlins, H. Shi, M. Jensen, and L. Morss, *Physica* 162-164C (1989) 97.
- [16] M. Murakami, N. Sakai, T. Higuchi, and S. I. Yoo, *Supercond. Sci. Technol.* 9 (1996) 1.
- [17] S. I. Yoo, N. Sakai, H. Takaichi, T. Higuchi, and M. Murakami, *Appl. Phys. Lett.* 65 (1994) 633.
- [18] S. I. Yoo, M. Murakami, N. Sakai, T. Higuchi, and S. Tanaka, *Jpn. J. Appl. Phys.* 33 (1994) L1000.
- [19] N. Sakai, S. I. Yoo, K. Sawada, T. Higuchi, N. Hayashi, F. Frangi, and M. Murakami. "Fourth Euro Ceramics" vol. 7 pp. 77-84 High Tc Superconductors, Edit by A. Barone, D. Fiorani, A. Tampieri.

- [20] W. Ting, T. Egi, K. Kuroda, N. Koshizuka, and S. Tanaka, *Appl. Phys. Lett.* 70 (1997) 770.
- [21] M. Nakamura, Y. Yamada, T. Hirayama, Y. Ikuhara, Y. Shionara, S. Tanaka, *Physica C* 259 (1996) 295.
- [22] R. H. Hammond, V. Matijasevic, and R. Bormann, "Science and Technology of Thin Film Superconductors 2" Edited by R. D. McConnell and R. Nuofi (1990) 395.
- [23] N. Chikumoto, J. Yoshioka, M. Otsuka, N. Hayashi, M. Murakami, *Physica C* 281 (1997) 253.
- [24] M. R. Koblishka, A. J. van Dalen, T. Higuchi, S. I. Yoo, and M. Murakami, *Phys. Rev. B* 58 (1998) 2863.
- [25] T. Egi, J. G. Wen, K. Kuroda, H. Unoki, and N. Koshizuka, *Appl. Phys. Lett.* 67 (1995) 2406.
- [26] M. Murakami, S. I. Yoo, T. Higuchi, N. Sakai, J. Welz, N. Koshizuka, and S. Tanaka, *Jpn. J. Appl. Phys.* 33 (1994) L715.
- [27] M. Kambara, X. Yao, M. Nakamura, Y. Shiohara, T. Umeda, *J. Mater. Res.* 12 (1997) 2866.
- [28] H. Wu, M. J. Kramer, K. W. Dennis, R. W. McCallum, *Physica C* 290 (1997) 252.
- [29] D. B. Chrisey and G.K. Hubler "Pulsed Laser Deposition of Thin Films" Wiley Interscience Publication (1994).
- [30] S. R. Foltyn, R. C. Dye, K. C. Ott, E. Peterson, K. M. Hubbard, W. Hutchinson, R. E. Muenchausen, R. C. Estler and X. D. Wu, *Appl. Phys. Lett.* 59 (1991) 594.
- [31] M. C. Foote, B. B. Jones, B. D. Hunt, J. B. Barner, R. P. Vasquez, and L. J. Bajuk, *Physica C* 201 (1992) 176.

- [32] F. F. Chen, "Introduction to Plasma Physics", Plenum, New York (1974), ch. 1.
- [33] D. B. Geohegan, "Laser Ablation of Electronic Materials Basic Mechanism and Applications" Edited by E. Fogarassy and S. Lazare, Elsevier Science Publishers B. V. (1992) 73.
- [34] Milton Ohring, "The Materials Science of Thin Films" Academic Press (1991) ch. 5.
- [35] R. Feenstra, T. B. Lindemer, J. D. Budai, and M. D. Galloway, J. Appl. Phys. 69 (1991) 6569.
- [36] T. B. Lindemer, F. A. Washburn, C. S. MacDougall, R. Feenstra, and O. B. Cavin, Physica C 178 (1991) 93.
- [37] M. Badaye, J. G. Wen, K. Fukushima, N. Koshizuka, T. Morishita, T. Nishimura, and Y. Kido. Supercond. Sci. Technol. 10 (1997) 825.
- [38] M. Badaye, Wu Ting, K. Fukushima, N. Koshizuka, T. Morishita, and S. Tanaka. Appl. Phys. Lett. 67 (1995) 2155.
- [39] X. Yao, M. Kambara, T. Umeda, Y. Shiohara, Physica C 296 (1998) 69.
- [40] H. Nozaki, S. Takekawa, and Y. Ishizawa Jpn. J. Appl. Phys. 27 (1988) L31.
- [41] Y. Iijima, N. Tanabe, O. Kohno, and Y. Ikeno, Appl. Phys. Lett. 60 (1992) 769; Y. Iijima, K. Onabe, N. Futaki, N. Sadakata, and O. Kohno, J. Appl. Phys. Lett. 74 (1993) 1905.
- [42] R. P. Reade, P. Burdahl, R. E. Russo, and S. M. Garrison, Appl. Phys. Lett. 61 (1993) 2231.
- [43] N. Sonnenberg, A. S. Longo, M. J. Cima, B. P. Chang, K. G. Ressler, P. C. McIntyre, and Y. P. Liu, J. Appl. Phys. 74 (1993) 1027.
- [44] A. Goyal, D. P. Norton, D. M. Kroeger, D. K. Christen, M. Paranthaman, E. D. Specht, J. D. Budai, Q. He, B. Saffian, F. A. List, D. F. Lee, E. Hatfield, P. M.

- Martin, C. E. Klaubunde, J. Mathis, C. Park. *Journal of Materials Research* 12 (1997) 2924.
- [45] J. I. Goldstein, D. E. Newbury, P. Echlin, D. C. Joy, A. D. Romig, Jr., C. E. Lyman, C. Fiori, E. Lifshin, in "Scanning Electron Microscopy and X-Ray Microanalysis" second edition (Plenum Press, New York, 1994).
- [46] F. Izumi, S. Takekawa, Y. Matsui, N. Iyi, H. Asano, T. Ishigaki, and N. Watanabe, *Jpn. J. Appl. Phys.* 26 (1987) L1616.
- [47] S. I. Yoo and R. W. McCallum, *Physica C* 210 (1993) 157.
- [48] S. Li, E. A. Hayri, K. V. Ramanujachary, and M. Greenblatt, *Phys. Rev. B* 38 (1988) 2450.
- [49] E. A. Goodilin, N. N. Oleynikov, E. V. Antipov, R. V. Shpanchenko, G. Yu. Popov, V. G. Balakirev, Yu. D. Tretyakov. *Physica C* 272 (1996) 65.
- [50] T. Itoh, M. Uzawa, and H. Uchikawa, *Phys. Lett. A* 129 (1988) 67.
- [51] J. Hauck, K. Bickmann, and K. Mika, *Supercond. Sci. Technol.* 11 (1998) 63.
- [52] M. J. Kramer, A. Karion, K. W. Dennis, M. Park, and R. W. McCallum, *Journal of Electronic Materials* 23 (1994) 1117.
- [53] T. Goto, T. Miura, and T. Hayashi, *Jpn. J. Appl. Phys.* 36 (1997) L909.
- [54] S. Gong, D. Shi, G. Zhou, C. Cai, Y. Fu, H. Zhang, *Physica C* 282-287 (1997) 469.
- [55] X. Obradors, R. Yu, F. Sandiumenge, B. Martinez, N. Vilalta, V. Gomis, T. Puig, and S. Pinol, *Supercond. Sci. Technol.* 10 (1997) 884.
- [56] T. Shimizu, H. Nonaka, and K. Arai, *Appl. Phys. Lett.* 59 (1991) 600.
- [57] N. Takahashi, N. Takeda, A. Koukitu, and H. Seki, *Jpn. J. Appl. Phys.* 36 (1997) L553.
- [58] H. U. Krebs, Ch. Krauns, X. Yang, and U. Geyer, *Appl. Phys. Lett.* 59 (1991) 2180

- [59] Y. Niiori, Y. Yamada, Y. Yoshida, and I. Hirabashi, *Jpn. J. Appl. Phys.* 35 (1996) L1407.
- [60] G. V. M. Williams and J. L. Tallon *Physica C* 258 (1996) 41.
- [61] S. Tsurumi, T. Iwata, Y. Tajima, and M. Hikita, *Jpn. J. Appl. Phys.* 27 (1988) L397.
- [62] D. V. Fomichev, O. G. D'yachenko, A. V. Mironov, E. V. Antipov, *Physica C* 225 (1994) 25.
- P. Diko, H. Kojo, M. Murakami, *Physica C* 276 (1997) 185.
- [63] H. Nonaka, T. Shimizu, and K. Arai, *Appl. Phys. Lett.* 57 (1990) 2850.
- [64] M. Badaye, F. Wang, K. Fukushima, and T. Morishita, *Supercond. Sci. Technol.* 8 (1995) 638.
- [65] Y. Ren, H. B. Tang, Q. W. Yan, P.L. Zhang, Y. I. Liu, C. G. Cui, T. S. Ning, Z. Zhang, and S. W. Niu, *Phys. Rev. B* 38 (1988) 11861.
- [66] F. Sandiumenege, N. Vilalta, J. Rabier, X. Obradors, *Appl. Phys. Lett.* 73 (1998) 2660.